Chapter 10

An *in silico* approach on the effects of phosphorylated (pY39, pS87 and pS129) α-Synuclein on the membrane protein interaction

An *in silico* approach on the effects of phosphorylated (pY39, pS87 and pS129) α-Synuclein on the membrane protein interaction

10.1. Abstract:

The biological function of α-Syn, which includes controlling synaptic vesicles, is regulated by phosphorylation at the Tyrosine 39 (pY39) residue. This function can be important for both normal and aberrant functions, and it relies on the interaction of α-Syn with the lipid membrane. Also, the phosphorylation at position Serine 87 (pS87) is increased in synucleinopathies, inhibits α-Syn oligomerization, and affects the interaction between α-Syn and the membrane. Phosphorylated α-Syn is present in relatively small levels in normal human brains, but nearly all of the α-Syn in the LB that collect in the nigrostriatal region in the brain of PD patients is phosphorylated on Serine 129 (pS129). Earlier studies suggested that mimicking phosphorylation at pS129 may have an inhibitory effect on α-Syn aggregation and thus control α-Syn neuropathology. Although phosphorylation at pS129 is associated with α-Syn inclusion in synucleinopathies, the mechanisms by which this PTM influences aggregation and contributes to LB illness in the brain are yet to be understood. Using MD simulations, this computational study has demonstrated the effect of PTM on the conformational dynamics of phosphorylated (pY39, pS87 and pS129) α-Syn and its lipid membrane association. To better understand the impact of pY39, pS87 and pS129 on the aggregation of the α-Syn structure monomer with recent atomic details, we have examined the MD trajectories, conducted a salt-bridge interaction study, PCA, and intra and inter-molecular hydrogen bond analysis. From the MD study, we have observed that phosphorylation at Tyr 39 position in α-Syn has a marked effect on its interaction with the lipid membrane. The conformational snapshots of α-Syn obtained showed a high degree of fluctuations in the N-terminal region that disrupts the helix-2 binding region. Phosphorylated pS87 α-Syn showed minimal flexibility and fluctuations and the amyloidogenic NAC region showed lower interaction with the membrane as well as within the different regions of the α-Syn structure. The conformational structure of pS129 α-Syn was observed from the MD trajectory analysis to be stable throughout the simulation, with higher compactness and reduced flexibility. The secondary structures of pS87 α-Syn was found to be retained influence the NAC region to immerse into the membrane while inhibiting the potential to interact with other neighbouring molecules. Further, the intermolecular hydrogen bonds analysis indicates that the NAC region is not embedded into the lipid bilayer and has limited association with the other regions of the protein. Our findings reveal salient features of pS129 modifications that inhibit α-Syn aggregation. Moreover, it was observed that in the case of

pS129 α-Syn as opposed to pY39 and pS87 α-Syn, there were larger energy disparities between the local and global minima of the overall structure.

10.2. Introduction:

The most frequent post-translational alteration of eukaryotic proteins is phosphorylation, which functions as a chemical switch to control interactions among proteins [586, 587]. The broad class of enzymes known as kinases are responsible for carrying out this activity [588], while phosphatases are responsible for its reversal activity [589]. Serine, Threonine, and Tyrosine are the most frequently phosphorylated amino acids, though arginine, lysine, aspartic acid, glutamic acid, and cysteine can also be phosphorylated on occasion. The binding of a phosphate atom to the hydroxyl group that comprises certain amino acid side chains occurs during the esterification process known as "phosphorylation" of proteins [586, 590]. Kinases are an important target for pharmaceutical therapy since they are linked to a multitude of human diseases, notably neurodegenerative disorders, because of the occurrence of protein phosphorylation [591, 592]. α-Syn undergoes diverse PTM states including acetylation, nitration, ubiquitination, glycosylation, and phosphorylation. LB and LN are produced at the synaptic terminals as a result of the abnormal accumulation and aggregation of α-Syn amyloid fibrils, one of the key pathological hallmarks of PD and other synucleopathies [55]. It is commonly recognized that PTM in proteins may be crucial in preventing the protein's ability to interact with biological membranes and membrane proteins, which are necessary for neurotransmitter release and synaptic formation [593]. More than 1% of demographic population over 60 years of age are affected by PD, the second most common chronic progressive neurological condition [594]. One of the main pathogenic characteristics of PD is the degradation of the dopaminergic nigrostriatal pathway, which impairs dopaminergic neurotransmission in the basal ganglia. Common pathological characteristics at post-mortem include the presence of dystrophic LN and aggregated α-Syn inside cytoplasmic LB [595]. LB development, fibrillogenesis, α-Syn aggregation, and neurotoxicity *in vivo* may all be regulated by phosphorylation at S87 [417, 554, 596, 597].α-Syn has been found to be constitutively phosphorylated at S87 (pS87) in cell cultures [172, 598] and animal models of PD studies [597, 599]. Patients with PD, AD, Lewy body disease (LBD), and multiple system atrophy (MSA), as well as the related transgenic (Tg) animal models, were shown to have considerably greater levels of pS87 in their brains [417,596, 597]. Recent findings also reported traces of p87 in human plasma and CSF. The important factor responsible for triggering fibrillogenesis and α-

syn aggregation *in vitro* as well as in cell culture, are localization of pS87 in the hydrophobic NAC region, [138,600-603]. It has been demonstrated that phosphorylation at pS87 residue has potent anti-aggregation effects by rendering α-Syn more structurally flexible and lowering its attraction for lipid membranes and vesicles [597]. Furthermore, a charged phosphate group may have an effect on the oligomerization, structure, and function of proteins [552]. pS129 is more common in LB patients as it increases from 4% in healthy individuals to 90% in LB sickness, indicating it is connected to the pathogenicity of the illness [596, 554, 604]. The effect stabilization or destabilization on the conformation of α-Syn may be dependent on the presence of an anion or cation [605] such as a negatively charged phosphate (PO_4^{2-}) group. The modification of pS129 neither increases nor decreases cellular toxicity nor α-Syn aggregation [606, 607]. Moreover, the addition of a charged phosphate group at pS129 may influence the structure, oligomerization, and function of the α-Syn protein [552]. The membrane protein interaction of α-Syn protein may be affected by phosphorylation at different positions in distinct ways. Since residue pS129 within the α-helical domain may have a greater impact on the attachments of the N-terminal of α-Syn and the resulting protein aggregation [608-612]. The rate of pathogenic protein aggregation and deposition is also accelerated by pS129, which has an adverse effect on neuronal function [613]. Because of the strong positive potential of the residue, its cognate kinase enzyme chooses to phosphorylate it in a negatively charged area, such as the C-terminal (both in solution and in the fibrils). *In vivo* studies of pS129 showed non-toxicity and may represent a neuroprotective mechanism that speeds up the removal of aggregated α-Syn [614]. In the interaction of lipid membrane with the phosphorylated α-Syn, a wide variety of factors can be impacted such as its binding mode, folding behaviour, interaction with subcellular localization or vesicles, and dissociation factors [615]. Patients with PD have been shown to have significantly higher amounts of pS129 α-Syn in their Cerebral Spinal Fluid than their respective control [616-620]. The normal function of α-Syn protein and its proteolysis may be controlled by phosphorylation at pS129, which might serve as a molecular switch [621-623]. It has been suggested that pS129 may be crucial in stress-induced synaptic plasticity because stress and other physiological stimuli have a close influence over the phosphorylation state of α-Syn [624]. The main risk factor for PD is age [625, 626], and aberrant accumulation of pS129 in synucleinopathy-affected brains [596, 554] and pS129 levels rising with age suggest that this PTM may be important in the origin of PD and other related disorders. As per recent studies, the occurrence of pS129 α-Syn after the early α-Syn buildup is believed to impede the further progression of the aggregation propensity and suppress cytotoxicity [627]. Furthermore, pS129 α-Syn has been utilized as a protein

abundance marker in recent studies to assess disease stringency and assess the correlation among the pS129 α-Syn abundance and its substantial illness duration, physiological limitations, or cell death are examples of clinical or pathological parameters [342]. At the C-terminal (residues 96–140), the synthesis of the substantially negatively charged phosphate group is fascinating. Previous studies have demonstrated that the C terminus of α-Syn and β-Syn contain negatively charged, aromatic, and hydrophobic residues that are stabilized by interactions resulting from the initial interaction [628]. Furthermore, pS87 α-Syn alteration was primarily found in glial inclusions, with some instances also showing cortical neuronal threads. But pS87 α-Syn can be considered as an early type PTM, since it is unlikely to yield more at the neuronal inclusions [617]. The physicochemical characteristics of α-Syn are modified by pS87 α-Syn phosphorylation, which results in decreased membrane binding and suppression of fibril formation [597]. In a recent work, it was highlighted that since pS87 is located in the NAC area, it is essential for triggering α-Syn fibrillation, which has a significant impact on α-Syn aggregation. According to recent studies, α-Syn's biological role of controlling synaptic vesicles is regulated by phosphorylation at the Tyrosine 39 residue. This function is dependent on α-Syn's interaction with the lipid membrane and can be significant for both normal and abnormal function [626]. Fibrillary protein inclusions known as LBs and Lewy neurites (LNs) are often seen in the brain and are used as disease markers. The primary component of LBs and LNs (α-Syn), occurs in fibrillary forms [629]. A significant number of LBs have phosphorylated α-Syn on Serine 129 [630, 631]. The α-Syn aggregation and cytotoxicity depend on the amyloidogenic NAC region. This area is folded by a secondary β-sheet structure [632]. Fibril assembly depends on a hydrophobic NAC region consisting of 12 amino acids (residues 71–82). This hydrophobic fragment tends to self-polymerize after being cut off from the rest of the molecule to produce highly lethal amyloid fibrils and encourage the fibrillation of the entire α-Syn protein [633]. However, in a recent study it was hypothesized that phosphorylated α-Syn at position 129 (pS129 α-Syn) exhibits a significant prevalence over unphosphorylated α-Syn in regions that are affected early, midway, and late in the disease progression [634]. While phosphorylation at pS129 is linked to α-Syn inclusion in synucleinopathies, the process by which additional PTM have an impact on aggregation and contribute to LBD in the brain are yet unknown [635]. In living organisms, α-Syn unfolded monomers interact, forming two types of dimers: stable anti-parallel dimers and propagating parallel dimers. The propagating dimers develops by incorporating unfolded monomers, leading to ring-like and larger oligomers. These ring-like oligomers interact with the membrane, forming pores that cause abnormal calcium influx [636]. From our earlier study

[637], we observed that the α-Syn dimer primarily adopts conformations that differ from fibrils. Furthermore, we identified hydrogen bonds and non-bonded contacts that contribute to the stabilization of the fibril structure. To further understand the pathological significance of (pY39, pS87 and pS129) α-Syn to LB illness, and the conformational dynamics of (pY39, pS87 and pS129) α -Syn on its association with lipid membranes were analyzed using all-atom MD simulation.

10.3. Materials and Methods:

10.3.1. Preparation of phosphorylated α-Synuclein structures:

The RCSB Protein Data Bank was used to obtain the initial α-Syn structure (PDB ID: 1XQ8) [457] for the MD simulation investigation. Using the xleap module of the AMBER18 software package [205], Tyrosine residues at positions 39 of α-Syn and Serine at position 87 and 129 of α-Syn were phosphorylated by adding a negatively charged phosphate (PO_4^{2-}) group.

10.3.2. Preparation of pY39, pS87 and pS129 α-Synuclein membrane bilayer complexes:

The CHARMM GUI was applied to the PPM server to predict the initial position of (pY39, pS87 and pS129) α-Syn protein in relation to the lipid-water interface using the CHARMM GUI as shown in **Figure 10.1**[220]. The rest of the steps involved in membrane bound phosphorylated α-Syn protein complex using CHARMM GUI was mentioned in section **4.3.1**

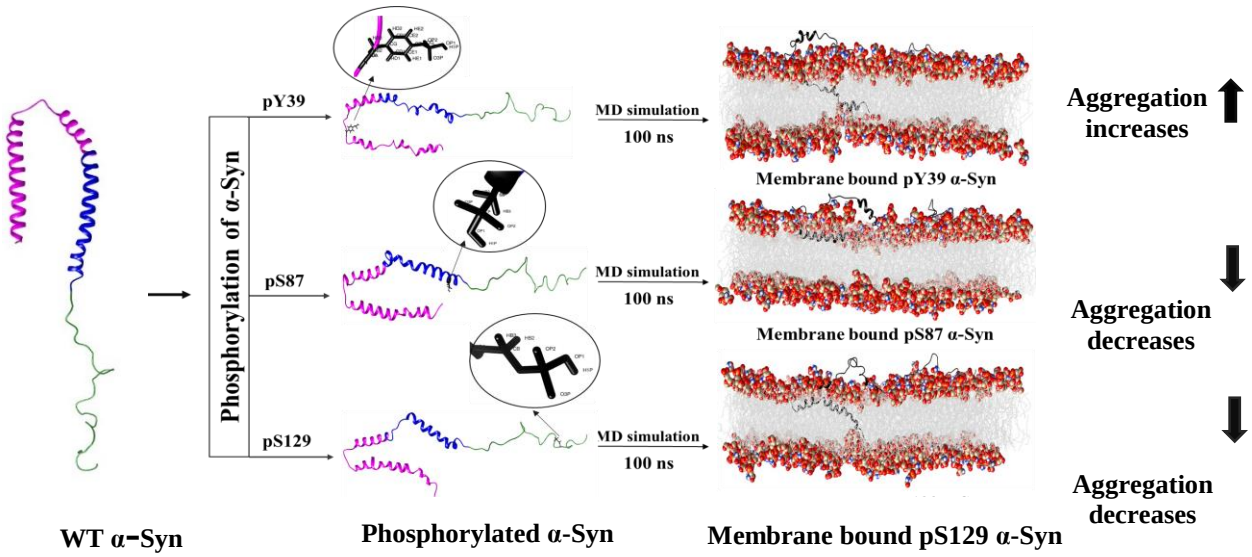

Figure 10.1. *Schematic representation of the phosphorylation of α-Syn at pY39, pS87 and pS129 followed by MD simulation*

10.3.3. Setup for MD simulations:

The assembled pdb file obtained from CHARMM GUI was then converted to AMBER formatted pdb file using charmm2lipid.py script. The MD simulation of the membrane-bound pY39, pS87 and pS129 α-Syn system was carried out using AMBER software version 18 and force fields (ff99SBildn and phosaa10) are used to generate topology and co-ordinate parameters in xleap module. The MD simulations were validated because of proper force field parameters such as ff99SBildn and lipid 17 and phosphorylated amino acid parameter such as phosaa10 are used for phosphorylation of α-Syn for analysing the molecular dynamics of IDP, which are characterised by rapid flexibility and dynamics with high amplitude, as well as the fact that limited aqueous volume effects of TIP4Pew water models were taken into account in MD simulations of IDPs in water. Followed by the MD steps that were mentioned in the module in section **4.3.2.**

10.3.4. Analysis of MD trajectories:

The stabilization of the membrane is the most important parameter before analyzing other structural features. The parameters that confirm its stability are EDP analysis of each component of the membrane bilayer (PC, PE, PS, oleoyl, water, and protein), EDP of each region of the protein, and the average area occupied by the lipid bilayer. The complex pY39, pS87 and pS129 α-Syn-lipid membrane system involved examining the lipid bilayer properties, including the lipid area, density profiles of lipid components, and thickness of the membrane. A time-averaged evaluation of the electron density throughout the lipid bilayer is provided by the electron density profile. Membrane thickness is the average of a phospholipid molecule of a single lipid layer and all the phospholipids of the other lipid layer [458]. The CPPTRAJ module [305] of the AMBER18 software package was used to carry out the following analyses from the corresponding MD simulation trajectories of 100 ns were investigated: RMSD and RMSF, Distance analysis between N-terminal and C-terminal domains of phosphorylated α-Syn, number of hydrogen bonds between different domains of α-Syn and lipid membrane, number of intramolecular hydrogen bonds of α-Syn. DSSP plots for the secondary structural content analysis using sander and Kabsch software [295] and calculation of percentage content of secondary structures using YASARA software [258]. The formation of salt bridges within the intramolecular residues was evaluated using the ESBRI server [259]. The plots derived from the MD trajectory analysis were constructed using xmgrace plotting tool.

10.3.5. Principal Component Analysis (PCA) along with free energy landscape:

PCA of conformers undergoing fluctuations is based on the eigenvectors of the mass-weighted covariance matrix (C), estimated on protein alpha carbons (C), using concatenated and MD trajectories, determines coordinated motion in MD trajectories of pY39, pS87 and pS129 α-Syn. The basic component free energy landscape was projected to comprehend the energy distribution throughout the protein folding process during MD simulation. The PCA analysis was performed that has been mentioned in section **8a.3.6.**

10.4. Results and Discussion:

10.4.1. Lipid surface area and thickness of the mixed lipid bilayer system:

The compactness of the phospholipid bilayer bound to phosphorylated (pY39, pS87 and pS129) α-Syn protein is determined by the area per lipid analysis as shown in **Figure 10.2**. Membrane thickness of the phosphorylated (pY39, pS87 and pS129) α-Syn protein was performed to understand the thickness of the bilayer system as shown in **Figure 10.3**. As a parameter, we utilized the average area per lipid to discover the equilibrium configurations of the DOPE/DOPS/DOPC mixed simulation system. By dividing the simulation box, lateral surface area by the total number of lipids in a leaflet, the area per lipid layer value was calculated. Each component of the membrane bilayer composed of PE, PC and PS showed higher density profiles as per the ratio of the composition (5:3:2). The biological importance of membrane dynamics in endocytosis and membrane remodelling highlighted the vitals for cellular homeostasis. These findings suggests the significance of understanding membrane dynamics for deciphering cellular mechanisms and developing therapeutic interventions [645]. In **Figure 10.2**, the area of the bilayer was observed to be stabilizing after 40 ns of the simulation time period. The average area for pY39 α-Syn was determined to be 64.22 $Å^2$ (Upper layer) and 66.69 $Å^2$ (Lower layer). On the contrary, the area per lipid bilayer of pS87 α-Syn was found to be 66.03 $Å^2$ (Upper layer) and 68.56 $Å^2$ (lower layer), which tends to be higher than pY39 α-Syn. **Figure 10.2** shows the time-dependent area per lipid profile for the mixed phospholipid bilayer. From the analysis, the Area per lipid analysis for the mixed bilayer lipid membrane (DOPE/DOPS/DOPC in 5:3:2) showed the following average of 67.5 Å2 for the upper layer and 70.1 $Å^2$ for the lower layer with respect to the time period.

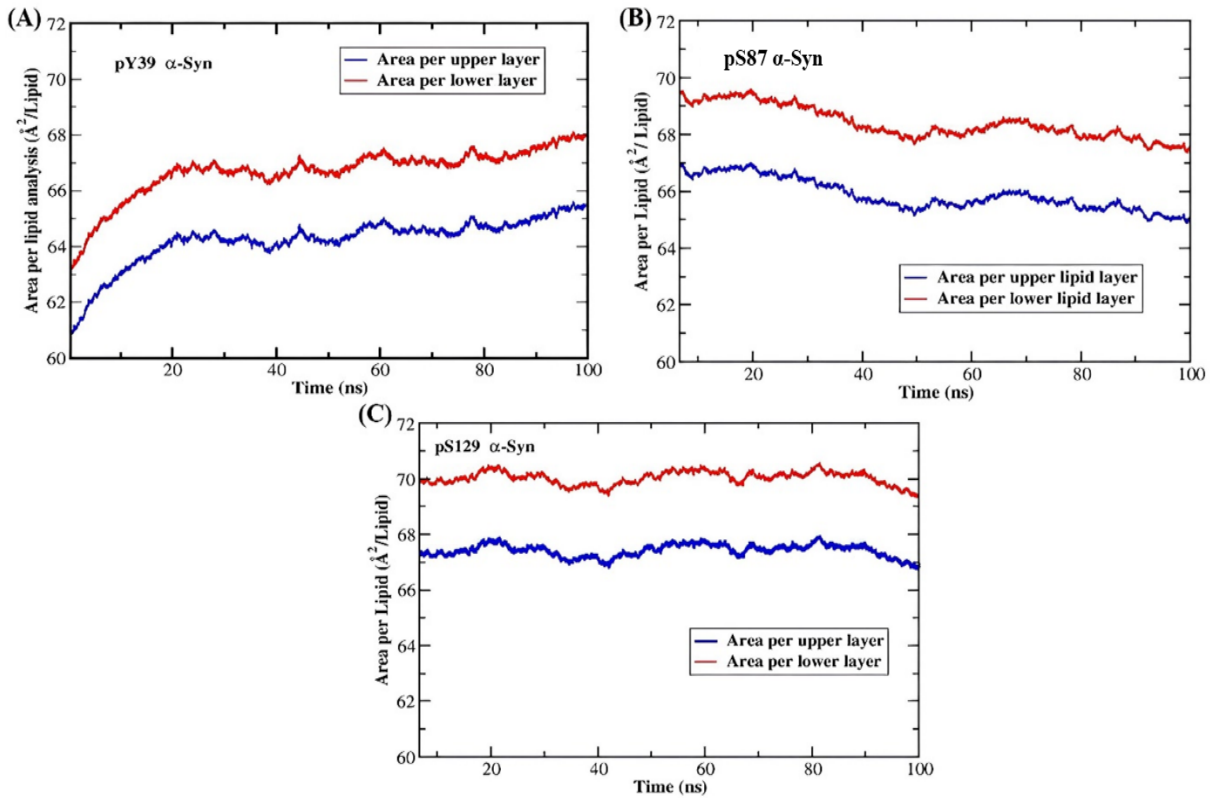

Figure 10.2. *Area per lipid bilayer of the phosphorylated α-Syn (A) pY39, (B) pS87 and (C) pS129 during MD simulation*

Furthermore, the average membrane thickness was assessed by measuring the shortest distance between a phosphorus atom in one leaflet of a lipid layer and every phosphorus atom in the other leaflet of the lipid layer. This measurement was utilized to determine the average membrane thickness [459, 460, 23]. In **Figure 10.3**, the plot depicting membrane thickness illustrates the temporal evolution of membrane thickness for DOPE/DOPS/DOPC mixed lipid bilayers, which remained stable over a simulated time of 100 ns. The calculated average membrane thickness was found to be 73.48 Å, 87.37 Å, and 89 Å for the pY39 α-Syn, pS87 α-Syn and pS129 α-Syn, respectively.

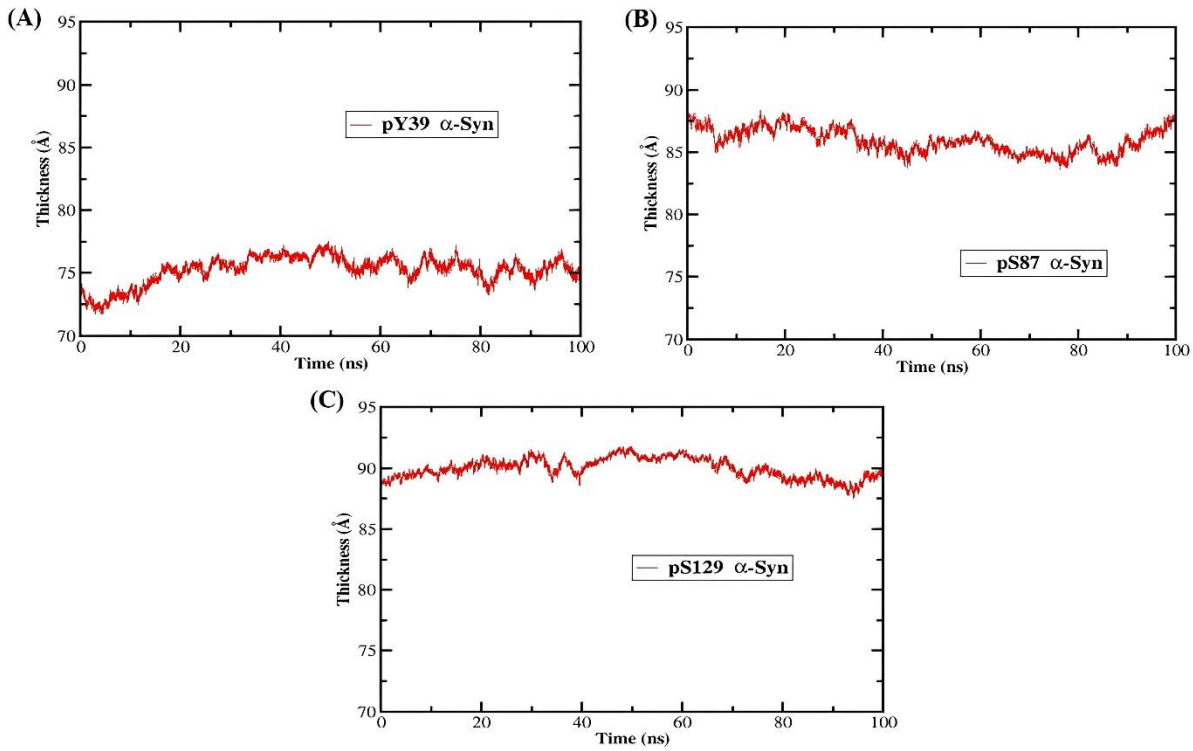

Figure 10.3. *Membrane thickness of the phosphorylated α-Syn (A) pY39, (B) pS87 and (C) pS129 during MD simulation*

10.4.2. Electron Density Profiles of the mixed lipid bilayer system:

Another important parameters including the EDP of each component of the phospholipid bilayer and individual domains of the α-Syn were plotted in **Figure 10.4** and **Figure 10.5**. In **Figure 10.4**, both the systems showed well-equilibration in the range ±20 Å for the entire simulated trajectories as a function of simulation time. However in the **Figure 10.5**, the density profile for each domain of pY39 α-Syn showed deep insertion of the N-terminal at 29 Å followed by the NAC domain and C-terminal embedded at 8 Å below the bilayer center (Z-axis). On the contrary, the depth of the N-terminal of pS87 α-Syn was found to be 20 Å while the NAC domain and C-terminal was buried at 12 Å and 14 Å respectively.

A bio-membrane density is determined by calculating the surface area of the entire lipid membrane system. In order to determine balanced conformation of the phospholipid di-oleoyl (PE, PS and PC) lipid membrane bilayer, the average surface area of the lipid bilayer was examined as a measure. To compute the area of the lipid bilayer, the whole area of the bilayer surface simulated box was divided by the total amount of lipids in a single leaflet.

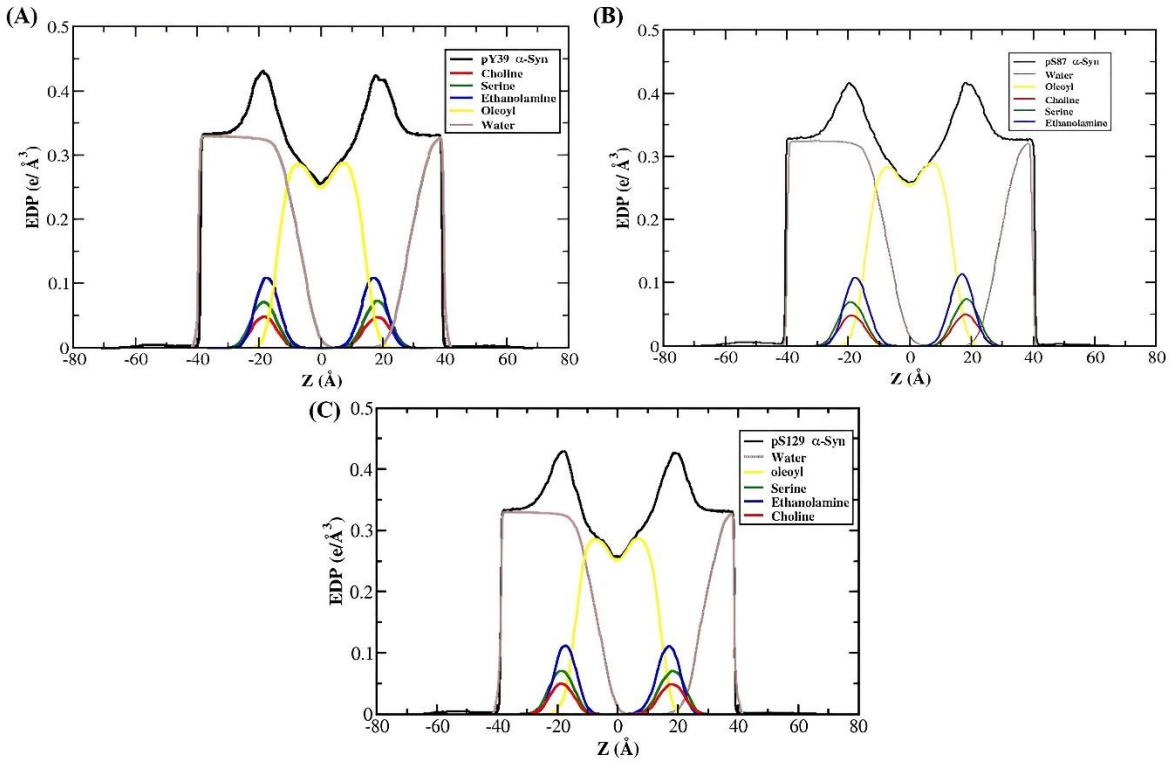

Figure 10.4. *Electron density plots of the phosphorylated α-Syn (A) pY39, (B) pS87 and (C) pS129 during MD simulation*

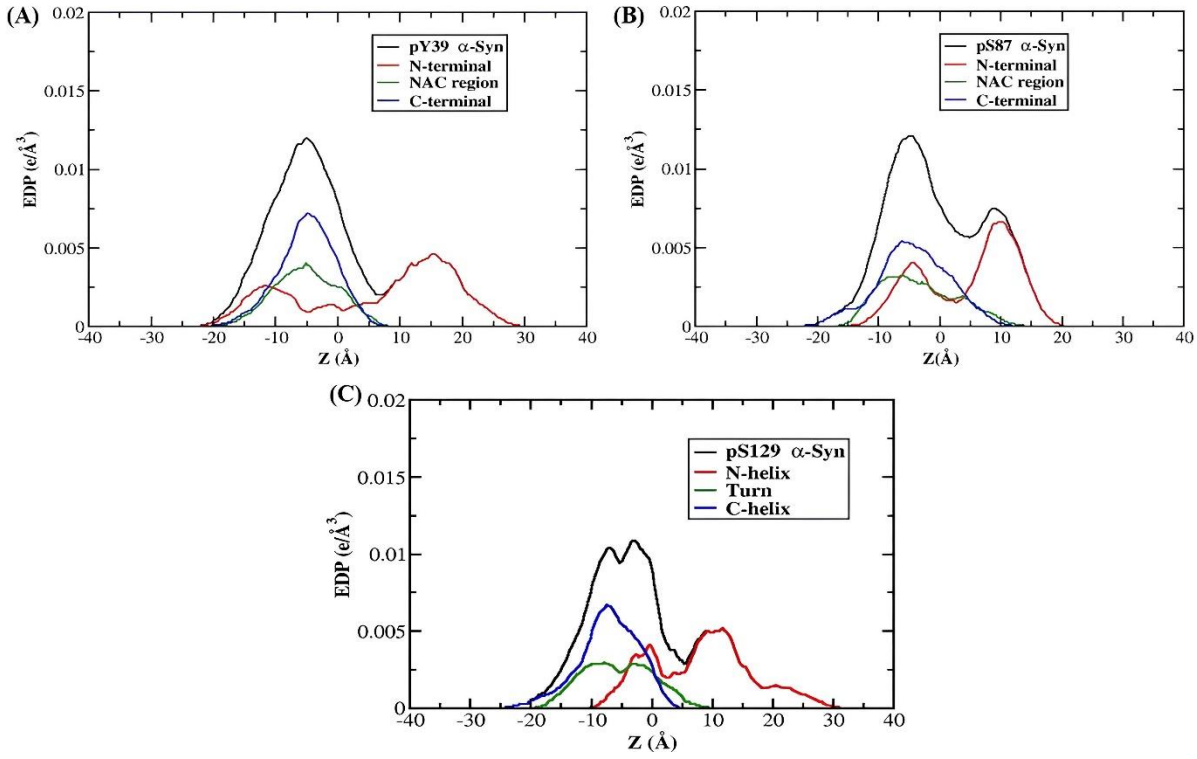

Figure 10.5. *Electron density plots of each component ofthe phosphorylated α-Syn (A) pY39, (B) pS87 and (C) pS129 during MD simulation*

10.4.3. RMSD analysis of the phosphorylated (pY39, pS87 and pS129) α-Synuclein complexes:

The measure of stability and degree of convergence of the phosphorylated pS129 α-Syn were assessed during the MD simulation using RMSD. In **Figure 10.6(A-C)**, it was observed that the backbone Cα RMSD values for pS129 α-Syn compared to their corresponding initial structure, which was determined from the MD simulation trajectories. It was shown that the structural conformation of the α-Syn structure changed quickly and that, after 50 ns, the conformation remained stable. The RMSD study was conducted during a simulated time of 100 ns on the different regions of phosphorylated pS129 α-Syn, as observed in **Figure 10.6 (C)**. It was noticed that the N-terminal and C-terminal of pS129 α-Syn undergo slight changes in conformation while NAC undergoes rapid changes in the conformational dynamics. The stability of the conformation of unphosphorylated α-Syn [547] was found to be lower in comparison with the stability of the conformation of phosphorylated α-Syn. The structural distance between two atomic coordinates that helps in measuring the displacement of a particular coordinate as a function of simulation time is determined as root mean square deviation or RMSD. For the pY39 α-Syn, its RMSD profile increases gradually and stabilizes at 6 Å during the simulation. But in the case of pS87 α-Syn, the RMSD showed an increase in the peaks upto 9.5 Å. From the **Figure 10.6(A)**, it was evident that the pY39 α-Syn was fairly stable than pS87 α-Syn. From our earlier study [638], the RMSD profile of unphosphorylated WT α-Syn was observed to undergo rapid change in the conformational dynamics and was found to have quite different and diverse RMSD profile as a function of simulation time period.

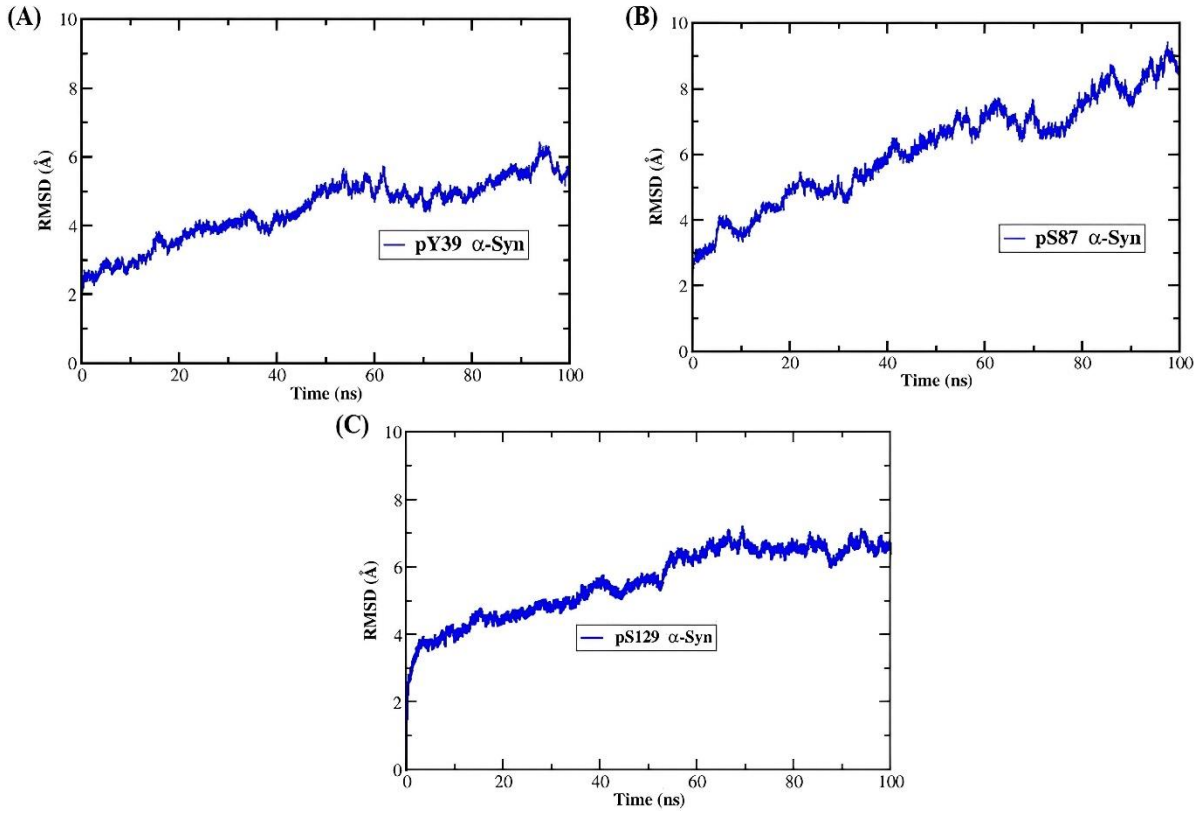

Figure 10.6. *RMSD analysis of phosphorylated α-Syn (A) pY39, (B) pS87 and (C) pS129 during MD simulation of 100 ns*

10.4.4. Free energy landscape profile followed by Principal Component analysis (PCA):

To analyze the simulated phosphorylated α-Syn system and assess the Cα atom after system stabilization of the MD simulation trajectories, free energy profile and PCA landscapes were employed. Global and local minima are provided by the first few major components. The eigenvectors (PC1 and PC2) are referred to as two-directional principal components (PCs) and included in the global minima of the protein structure. To illustrate the sampling space of the protein systems, the eigenvectors created a free energy profile. The RMSD profile (**Figure 10.6**) and the small variation in the pS129 α-Syn eigenvalues as observed in **Figure 10.7** both demonstrate that this compound appears to form stable conformers to occupy the least profile space. The size and shape of the minimum energy region provides information about the stability of the structure. Since the thermodynamically most stable structure lies at the minimum value of the free energy surface (ΔG), a more concentrated black region indicates a higher stability of the corresponding structure during the MD simulation. In **Figure 10.7**, the black colour indicates the lowest energy, and the purple colour indicates the meta-stable states of the conformer. In each system, one global minima followed by other subsidiary minima

structures was discovered. Nonetheless, it was indicated that there were fewer than 1.5 kcal/mol of energy differences between the secondary minima and the overall structure. As a result, simulated structures are highly flexible and have only a single primary form [57, 58]. The Free energy landscape was plotted in 2-D space to analyze the conformations that verified the same energy basin as characterized in the 3-D space as observed in **Figure 10.7**. The stability of the system after stimulation was determined by two parameters- the global and local minima conformations. The two eigenvectors (PC1 and PC2) are part of the global minima of the protein structure and are known as two-directional principal components (PCs). The protein complex sample space was shown by the eigenvectors free energy profile. The pY39 α-Syn showed single black dots indicating lowest energy surrounded by meta-stable states (purple) followed by 3-D space showing minimal basin depth. For the pS87 α-Syn (**Figure 10.7(B)**), the 2-D space showed multiple lowest energy profiles and higher range of eigenvectors were observed indicating higher instability of the structure. Furthermore, it was noticed that the energy differences between the local minima and the global minima of the overall structure was higher in the case of pS129 α-Syn than pY39 and pS87 α-Syn [295, 296].

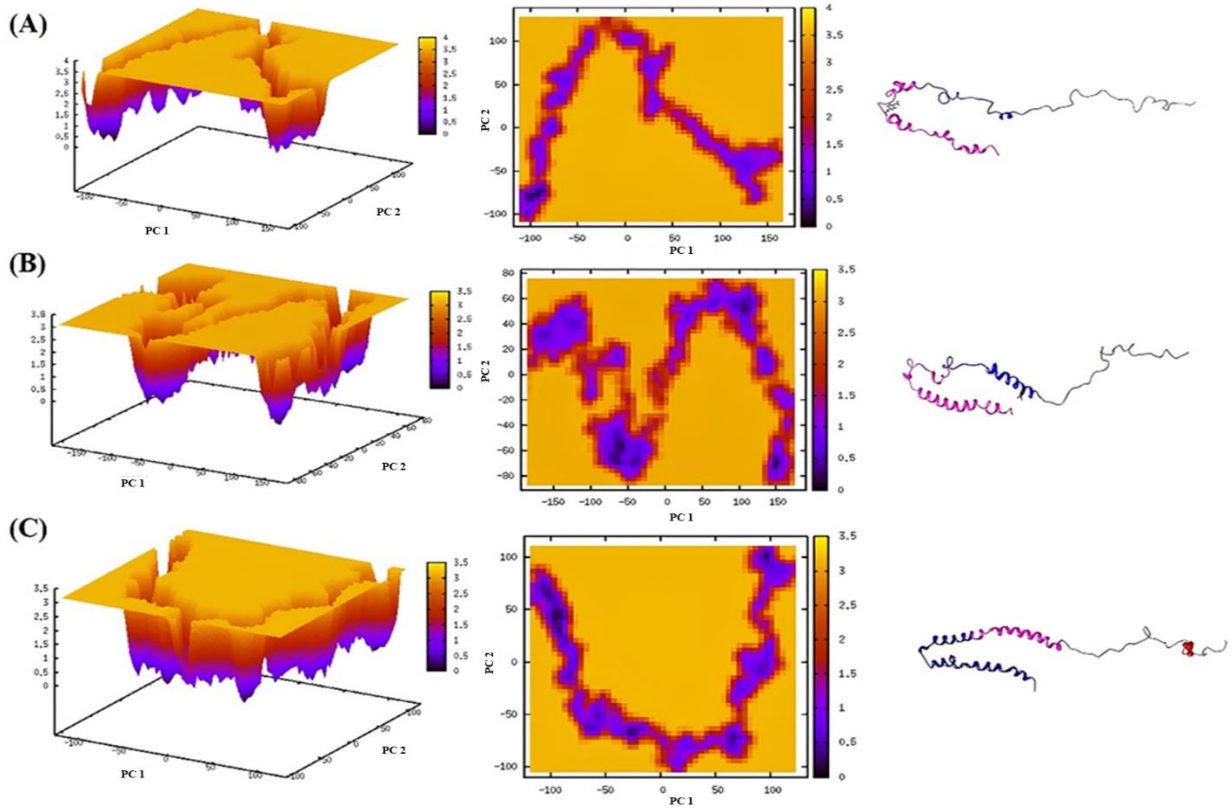

Figure 10.7. *PCA followed by 2D and 3D free energy landscapes (FEL) analysis of (A) pY39, (B) pS87 and (C) pS129 α-Syn. X, Y, and Z indicate PC1, PC2, and free energy, respectively. In the energy well, reflects the global minimum of all the phosphorylated α-Syn structures*

10.4.5. RMSF analysis of phosphorylated α-Synuclein complexes:

In order to assess individual residue flexibility, throughout the duration of the MD simulation, the RMSF values of all Cα atoms for the pS129 α-Syn were calculated and plotted in **Figure 10.8.** From **Figure 10.8**, the phosphorylation at residue pS129 α-Syn is the main causative factor for the descent in the C-terminal domain. Except at the site of phosphorylation, the protein showed slight fluctuation due to steric constraints from the site of phosphorylation. As a result, the phosphorylation at pS129 α-Syn residue decreases its fluctuation in the protruded region and also in the adjacent region. Hence, the overall lowering in the flexibility of pS129 α-Syn indicates that it can hinder membrane-protein interaction. The residual fluctuation of pY39 α-Syn was observed to have higher residual fluctuations of 4.2 Å in the ranges of 70-80 residue index and 105-120 residue index. Similarly, the RMSF profile of pS87 α-Syn showed higher residual fluctuations of 6 Å in the range of 70-80 residue index, and lower fluctuations were also observed in the residue ranges of 115-135. The RMSF profile of pS129 α-Syn showed higher residual fluctuations of 4.4 Å in the range of 65-80 residue index. The results obtained from RMSF analyses corroborate that the pS87 α-Syn showed higher structural instability.

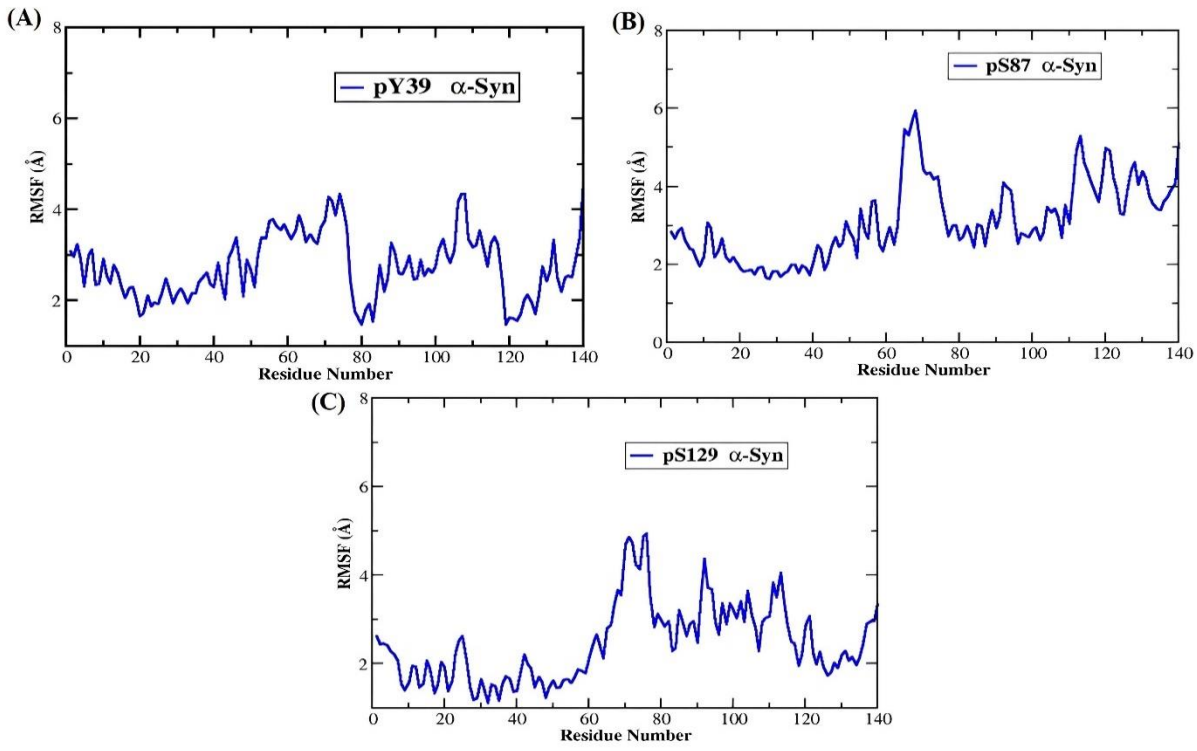

Figure 10.8. *RMSF analysis of phosphorylated α-Syn (A) pY39, (B) pS87 and (C) pS129 during MD simulation of 100 ns*

10.4.6. Radius of gyration analysis of phosphorylated α-Synuclein complexes:

Rg measures the total distance between each atom in a particular biomolecule and its center of gravity or common axis. The structural compactness of a protein is determined by Rg analysis. From **Figure 10.9**, the pS129 α-Syn showed have decrease in the Rg value range at different intervals of the simulation time that suggested greater compactness. In **Figure 10.9**, the N-terminal region, NAC region, and C-terminal region with Rg values present a constant probability range over a simulation time of 100 ns. However, it was noted that structures with higher Rg values are more exposed to solvent exposure and may aggregate more readily [636]. Therefore, the NAC region of pS129 α-Syn displayed the lowest value for Rg in our investigation, indicating that it is preventing α-Syn aggregation.

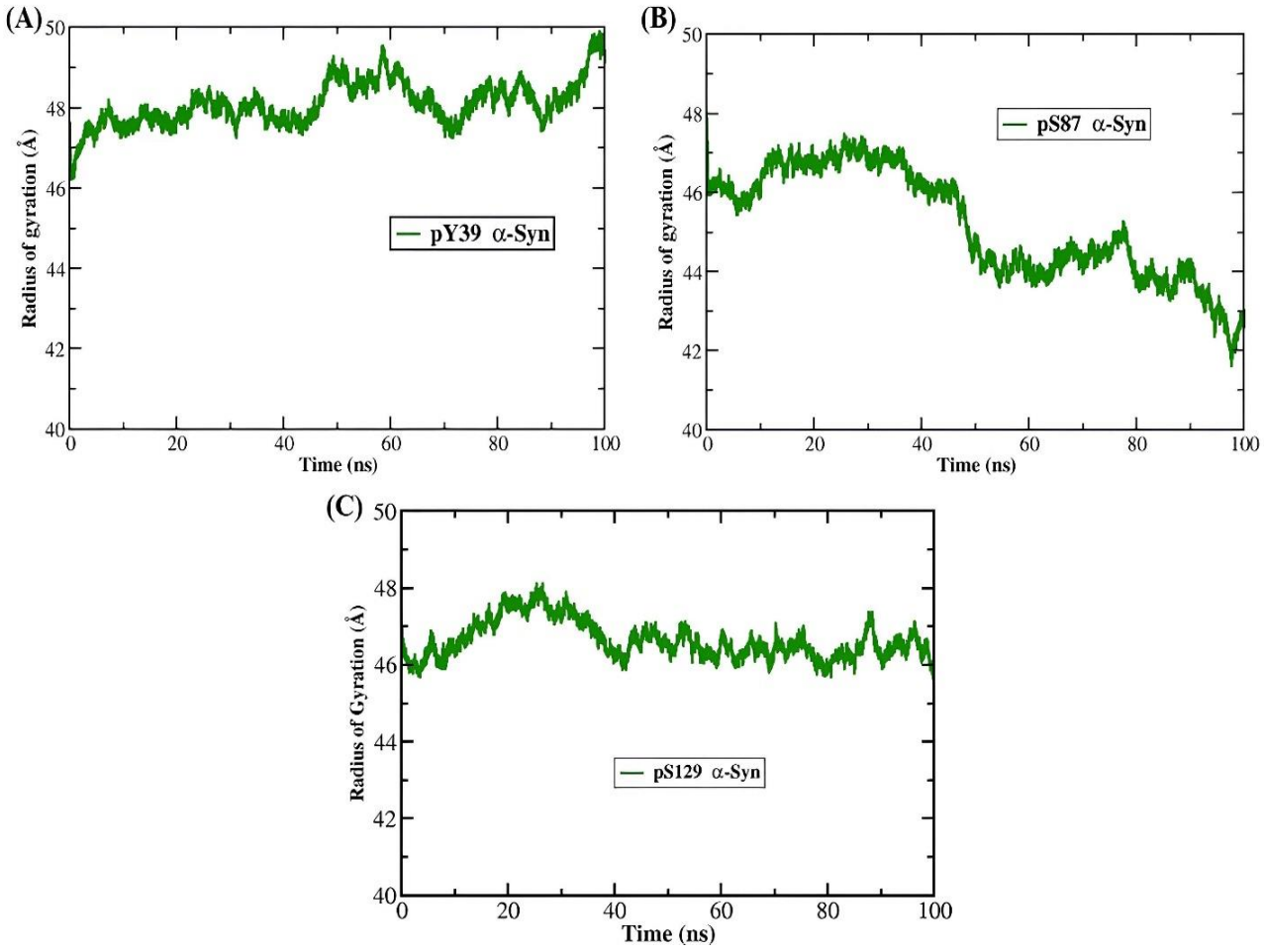

Figure 10.9. *Radius of gyration analysis of phosphorylated α-Syn (A) pY39, (B) pS87 and (C) pS129 during MD simulation of 100 ns*

10.4.7. Secondary structural analysis of phosphorylated α-Synuclein complexes:

The DSSP graph of the secondary structure derived from the MD trajectories was examined and plotted using the Kabsch and Sander technique. The probable secondary structures of each region of pS129 α-Syn were shown in **Figure 10.10,** the probable secondary structures of the complex were analyzed based on the trajectories that were obtained and determined the change in residue during the simulation trajectory analysis. As the simulation duration approaches, the helical composition is maintained in the pS129 α- Syn. Therefore, the NAC (hydrophobic) domain of pS129 α-Syn displayed the lowest value for Rg in our investigation, indicating that it is preventing α-Syn aggregation. In the median structure of pS129 α-Syn, the percentage secondary structure content for the average structure was calculated using YASARA software [258], and the details were summarized in **Table 10.1**. In this study, we noticed pS129 α-Syn to preserve the continuous helical conformation on the N-terminal (1-60) and NAC domain (61-95) to sustain the monomeric form. The percentage secondary structures determine the structural content (α-helix, β-sheets, 3-10 helix, Pi helix, Turn, and Coil) of phosphorylated (pY39 and pS87) α-Syn using Kabsch and Sander algorithm in the form of DSSP plot. In **Figure 10.10,** the DSSP plots of both the phosphorylated systems were depicted respectively. The percentage of secondary structural content calculated using YASARA was tabulated in Table 1. The percentage of α-helix was observed to be higher in pS129 and pS87 α-Syn than pY39 α-Syn suggests that pS129 and pS87 has retained its α-helical conformations. Also, other secondary structural contents of Turn and Coil were found to be higher in pY39 α-Syn suggests the breakdown of the helix-2 region.

***Table 10.1**. Secondary Structural content of pY39, pS87 and pS129 α-Syn after the simulation time using YASARA software*

COMPLEX	α-helix %	β-sheet %	turn %	Pi-helix %	3_{10} helix %	Coil %
pY39 α-Syn	11.4	1.4	34.3	0	2.9	50
pS87 α-Syn	29.3	1.4	25.7	0	0	43.6
pS129 α-Syn	30	0.7	25.7	0	0	43.6

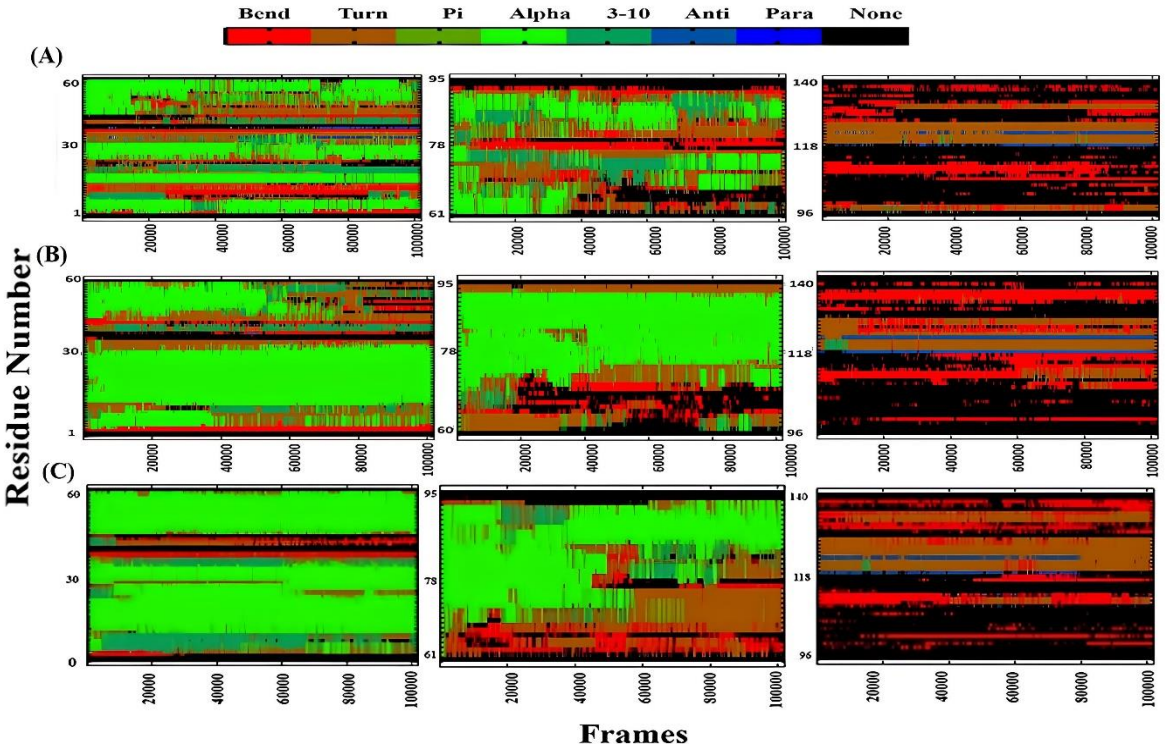

Figure 10.10. *DSSP plot of the phosphorylated α-Syn (A) pY39, (B) pS87 and (C) pS129 using Kabsch and Sander Algorithm*

10.4.8. Analysis of the Conformational Dynamics of phosphorylated α-Synuclein complexes:

The MD trajectories corresponding to the pS129 α-Syn snapshots associated with the lipid membrane are depicted. Particularly, the C-terminal has minimal contact with the membrane, the N-terminal is embedded into the lipid membrane, and the NAC hydrophobic region is raised above the lipid bilayer. In unphosphorylated α-Syn [547], we observed the NAC region protruding out from the membrane surface and also the reduction in the helical content in the region (45–95). In a recent study, it was reported that a single α-Syn molecule can connect and bridge two vesicles that are as far apart as 150 Å, with both the core region of α-Syn (residues 65–97) and the N-terminal anchor area (including 25 residues) adopting the conformational amphipathic α-helices. These data therefore provide a structural basis for the mechanism by which α-Syn promotes vesicle-vesicle interactions [424]. The potential role of the highly acidic region of α-Syn as an intramolecular consort is suggested, as it could shield the hydrophobic NAC domain, thereby preventing aggregation [639-641]. The central portion of the NAC region (amino acids 71–82), which is hydrophobic, is necessary for fibril formation. The fibrillation of α-Syn is induced by this 12-amino acid fragment (residues 71–82) self-polymerizes and forms lethal amyloid fibrils [620]. Since both the right-handed (α-Right) and left-handed (α-Left)

helical sections were oriented on their respective sides, as illustrated in **Figure 10.11**, it was evident that in the region 71–82, the α-strand was absent. The Ramachandran plot as observed in (**Figure 10.11(B)**) demonstrates a complete rearrangement of the right-handed and left-handed helical α-Syn structure on both sides. In a study [642], it was found that phosphorylation of α-catenin at specific sites significantly reduced the mechanical stability of the α-catenin/β-catenin complex. Phosphorylated α-catenin exhibited a lower resistance to mechanical force compared to the non-phosphorylated form, indicating that phosphorylation weakens the interactions within the complex. From our findings similar results was observed as phosphorylation at Tyr39 (pY39) α-Syn showed decrease in proximity within the N-terminal and NAC region. In a recent study [643], it was revealed that biochemical perturbations induce significant alterations in the conformational landscape of monomeric α-Syn. Additionally, the presence of specific molecules, such as lipid membranes could stabilize or destabilize certain structural intermediates, modulating the protein's behaviour. Similar results were observed in our study, as pY39 showed a high degree of fluctuation in the N-terminal region while pS87 undergo bending of the region near the site of phosphorylation that causes the C-terminal to flank out of the lipid membrane.

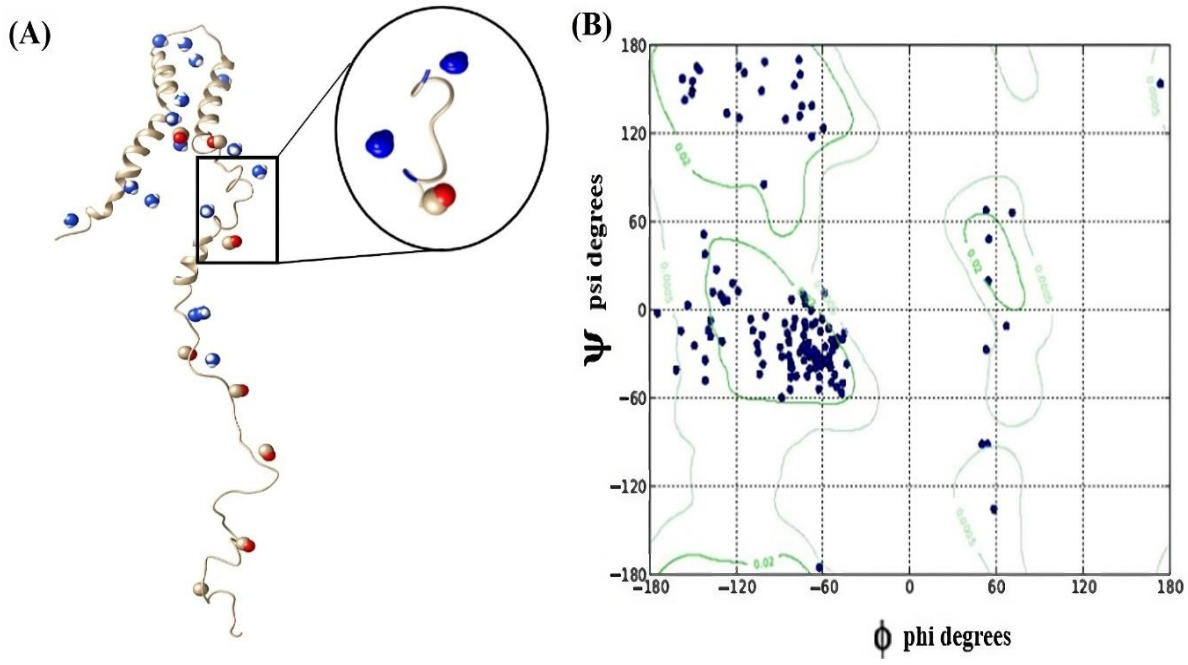

Figure 10.11. *(A) Conformational snapshots of phosphorylated pS129 α-Syn throughout the MD simulation time and (B) Ramachandran plot (ϕ, ψ) showing right-handed (α_R) and left-handed (α_L) helical regions*

The conformational snapshots of the 3-D structures of the phosphorylated (pY39, pS87) α-Syn were obtained from the MD trajectories as shown in **Figures 10.12-10.14**. The snapshots of pY39 α-Syn showed a high degree of fluctuation in the N-terminal region resulting in the disruption of the helix-2 binding region and thereby affecting the binding to the lipid bilayer. The proximity between the N-terminal and NAC region of pY39 α-Syn decreases due to the phosphorylation. The α-Syn fibril structure is completely rearranged as a result of pY39 α-Syn attraction to the lysine residues at the α-Syn N-terminal, which forms a hydrophilic channel in the core of the α-Syn protofilament [167]. While pS87 α-Syn was noticed to undergo bending of the region at the site of phosphorylation that causes the C-terminal to flank out of the lipid membrane consequently decreasing its binding affinity towards the membrane. The phosphorylation of pS87 α-Syn occurs in the hydrophobic NAC domain which is responsible for mediating fibrilization that subsequently affects α-Syn aggregation.

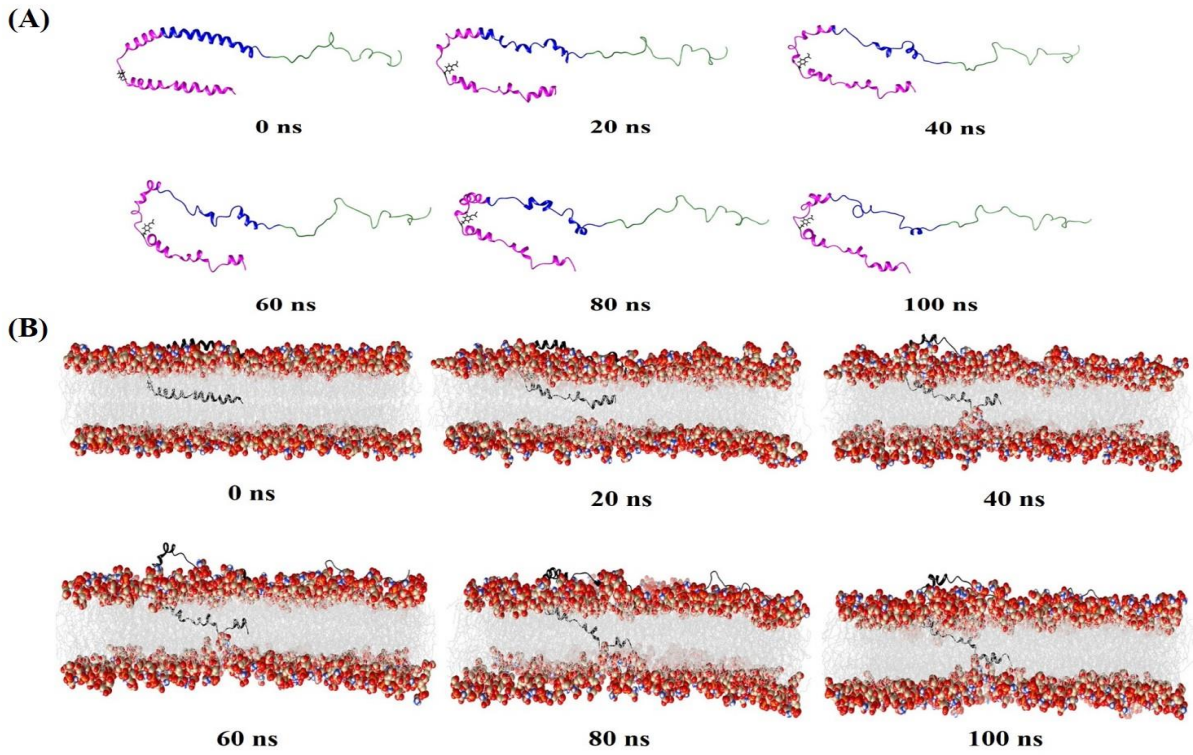

Figure 10.12. *Conformational Snapshots of the phosphorylated (pY39) α-Syn (A) membrane hidden and (B) membrane bound as a function of simulation time*

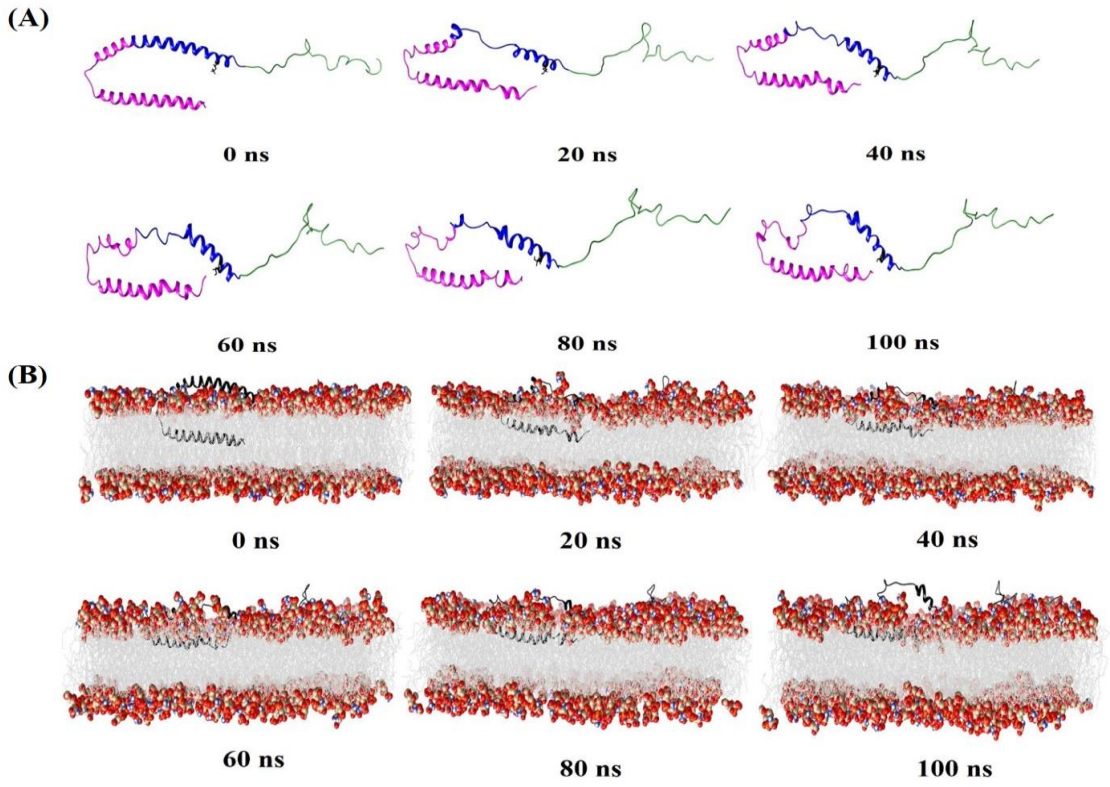

Figure 10.13. *Conformational Snapshots of the phosphorylated (pS87) α-Syn (A) membrane hidden and (B) membrane bound as a function of simulation time*

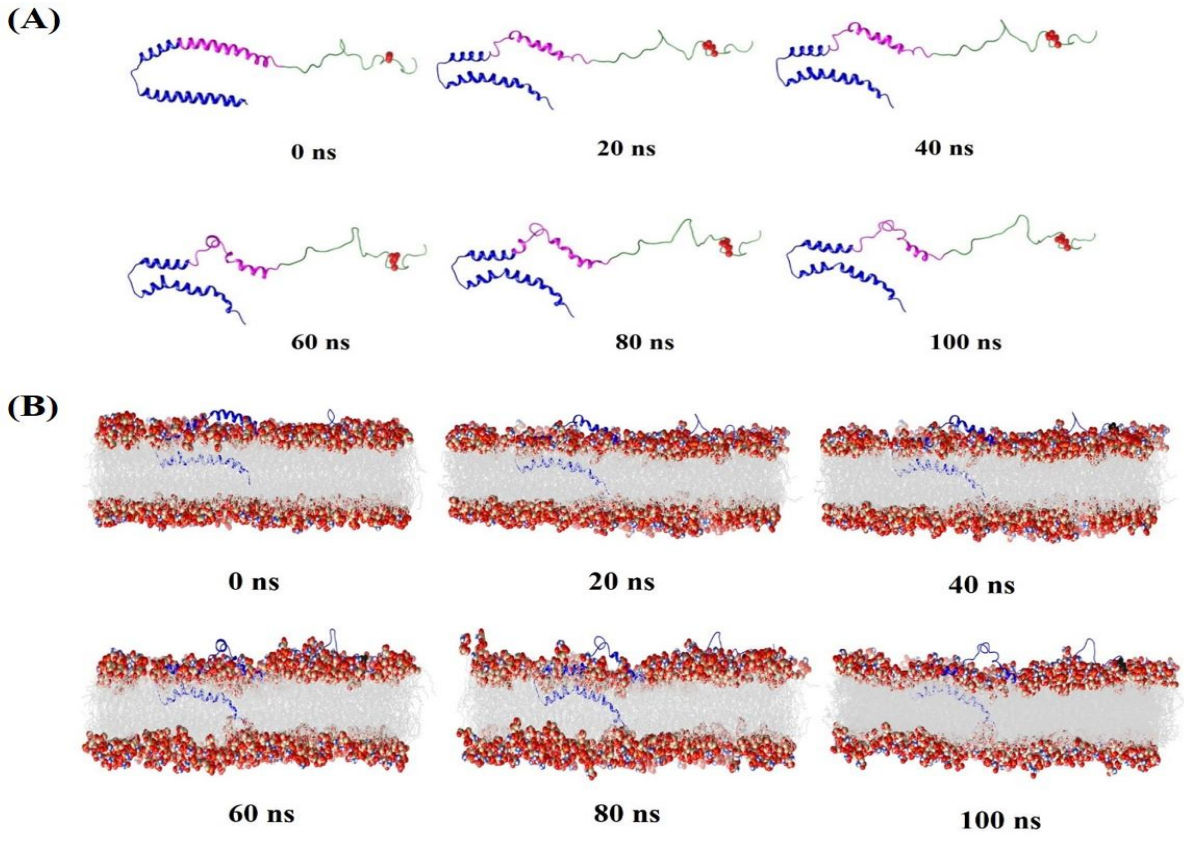

Figure 10.14. *Conformational Snapshots of the phosphorylated (pS129) α-Syn (A) membrane hidden and (B) membrane bound as a function of simulation time*

10.4.9. Hydrogen bond formation between phosphorylated α-Synuclein and lipid membrane:

To analyze the number of hydrogen bonds between the phosphorylated α-Syn and lipid membrane, the intermolecular hydrogen bond analysis was performed. In **Figures 10.15-10.17**, it was observed that the number of hydrogen bonds between the N-terminal of pS87, pS129 and the lipid membrane was slightly higher than pY39 followed by similar results of the hydrophobic NAC region. However, the C-terminal domain of pY39 α-Syn showed a higher number of intermolecular hydrogen bonds that contribute to the unfolding of the protein structure and enhance aggregation kinetics. In **Figure 10.17**, the number of inter-molecular hydrogen bonds between the N-terminal and C-terminal of pS129 α-Syn and lipid membrane was observed to be higher in comparison to the NAC region. This suggests that the NAC region was not buried into the lipid membrane but instead flanked out of the membrane surface. The tendency of pS129 α-Syn to aggregate upon binding to the lipid membrane determines the strength of association between the pS129 α-Syn and lipid membrane in forming the interaction. The atomistic level details regarding the intermolecular hydrogen bonds between the lipid bilayer as an acceptor or donor and phosphorylated (pY39, pS87 and pS129) α-Syn as an acceptor or donor were summarized in **Tables 10.2-10.7** respectively.

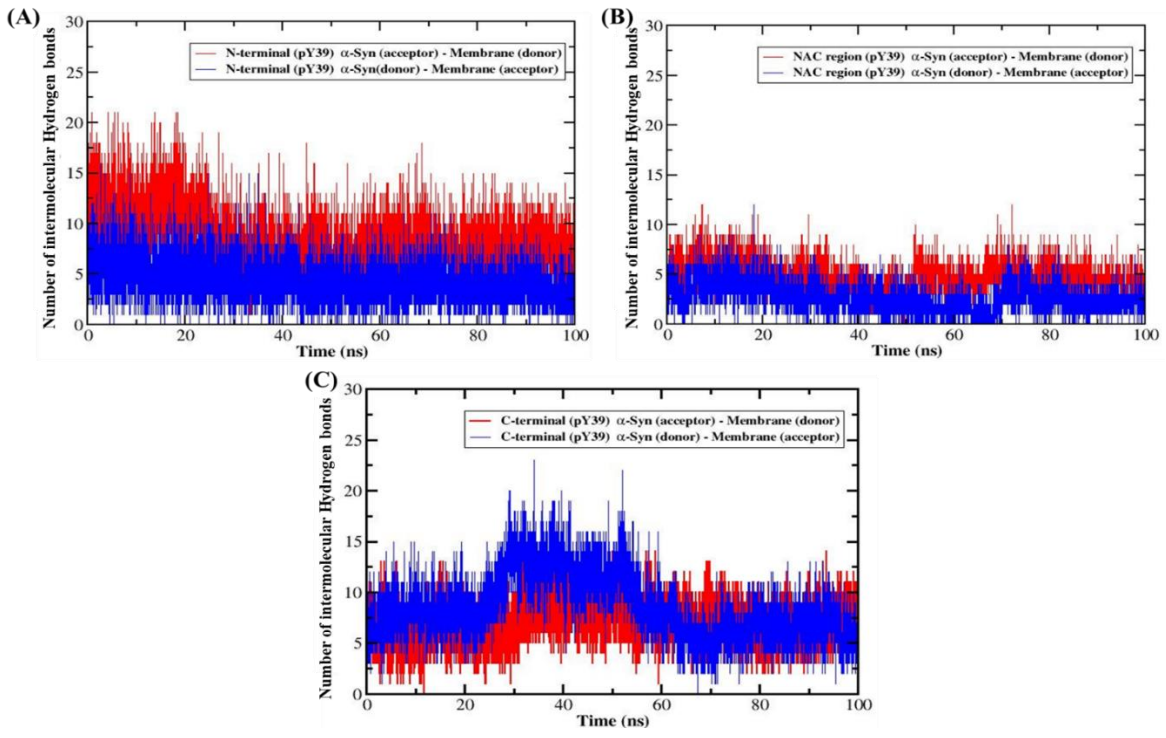

Figure 10.15. *Intermolecular hydrogen bond analysis between (A) N-terminal, (B) NAC region and (C) C-terminal of the phosphorylated α-Syn pY39 and lipid membrane during MD simulation*

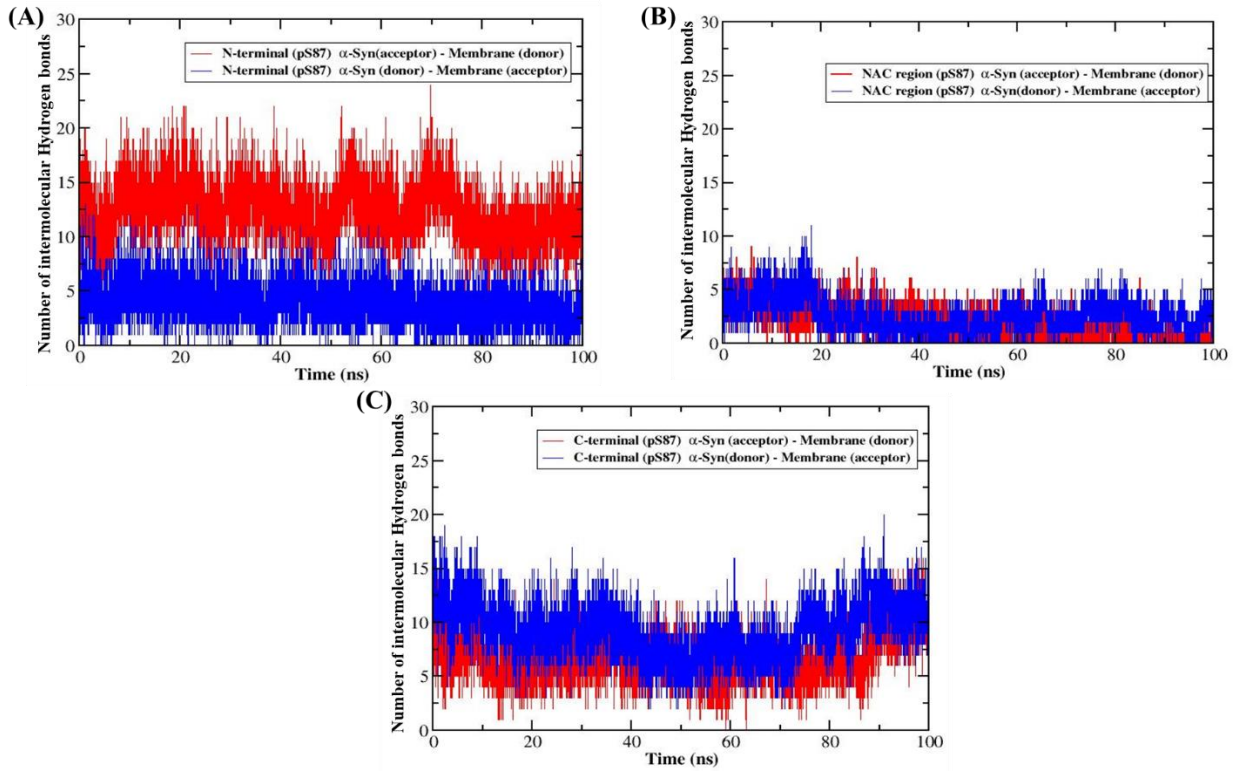

Figure 10.16. *Intermolecular hydrogen bond analysis between (A) N-terminal, (B) NAC region and (C) C-terminal of the phosphorylated α-Syn pS87 and lipid membrane during MD simulation*

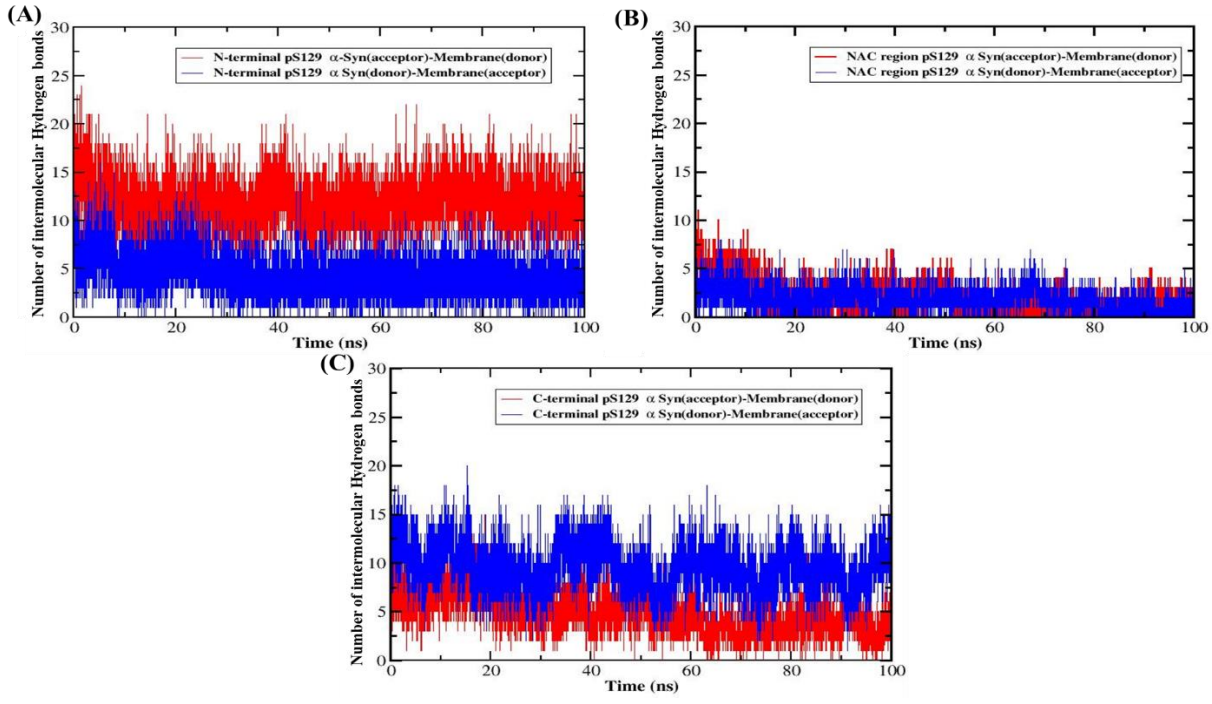

Figure 10.17. *Intermolecular hydrogen bond analysis between (A) N-terminal, (B) NAC region and (C) C-terminal of the phosphorylated α-Syn pS129 and lipid membrane during MD simulation*

Table 10.2. *Intermolecular Hydrogen bond analysis of membrane bound pY39 α-Syn during the MD simulation of 100 ns with membrane bilayer as acceptor and pY39 α-Syn as donor*

#Acceptor	DonorH	Donor	Average Distance (Å)	Average Angle (º)
PC_1705@O33	TYR_136@HH	TYR_136@OH	2.6308	165.6425
PC_1705@O12	GLN_134@HE22	GLN_134@NE2	2.8074	159.2191
PS_1813@O35	ASN_122@HD22	ASN_122@ND2	2.7758	156.8575
PS_1750@O35	LYS_80@H	LYS_80@N	2.8322	160.433
PC_1783@O34	SER_87@HG	SER_87@OG	2.6604	165.9093
PE_1732@O12	GLY_101@H	GLY_101@N	2.8441	153.6093
PS_1750@O35	GLN_79@H	GLN_79@N	2.8069	157.3742
PE_1714@O12	LYS_97@HZ2	LYS_97@NZ	2.7689	154.4207
PS_1750@O36	LYS_80@H	LYS_80@N	2.8341	161.1208
PS_1750@O36	LYS_80@HZ2	LYS_80@NZ	2.7263	157.2324
PS_1750@O35	THR_81@HG1	THR_81@OG1	2.6216	162.7535
PS_1750@O36	GLN_79@H	GLN_79@N	2.837	159.5233
PS_1750@O36	LYS_80@HZ3	LYS_80@NZ	2.7342	160.5493
PE_1735@O34	LYS_80@HZ3	LYS_80@NZ	2.7655	159.5078
PE_1735@O34	LYS_80@HZ1	LYS_80@NZ	2.7475	160.7485
PE_1714@O12	LYS_97@HZ1	LYS_97@NZ	2.7633	153.938
PE_1714@O12	LYS_97@HZ3	LYS_97@NZ	2.7591	154.2507
PS_1795@O36	LYS_43@HZ2	LYS_43@NZ	2.7848	157.2476
PE_1729@O33	LYS_21@HZ3	LYS_21@NZ	2.7649	155.7806
PE_1702@O34	GLN_62@HE21	GLN_62@NE2	2.7911	159.0402
PE_1858@O34	LYS_45@HZ1	LYS_45@NZ	2.7287	160.2699
PE_1711@O33	THR_44@HG1	THR_44@OG1	2.6794	161.1996
PS_1789@O35	ASN_65@HD21	ASN_65@ND2	2.8027	158.4463
PC_1870@O12	ASN_103@HD22	ASN_103@ND2	2.8409	161.0668
PS_1747@O35	LYS_102@HZ1	LYS_102@NZ	2.7925	155.981
PE_1729@O33	LYS_21@HZ1	LYS_21@NZ	2.758	154.5283
PC_1777@O31	Y1P_39@H1P	Y1P_39@O1P	2.846	150.5466
PE_1729@O33	LYS_21@HZ2	LYS_21@NZ	2.7618	154.1717
PE_1735@O33	LYS_80@HZ3	LYS_80@NZ	2.7475	158.6947
PE_1825@O12	SER_42@HG	SER_42@OG	2.719	160.6058
PE_1765@O33	LYS_96@HZ1	LYS_96@NZ	2.7561	156.4149
PC_1855@O12	LYS_80@HZ1	LYS_80@NZ	2.7746	151.4474
PS_1813@O36	ASN_122@HD22	ASN_122@ND2	2.7785	152.461
PE_1765@O22	GLN_99@HE21	GLN_99@NE2	2.8218	159.7347
PE_1828@O33	THR_72@HG1	THR_72@OG1	2.7324	160.5917
PS_1750@O12	SER_87@HG	SER_87@OG	2.6663	162.1586
PS_1747@O36	LYS_102@HZ1	LYS_102@NZ	2.7903	153.7459

PE_1732@O34	ASN_103@HD22	ASN_103@ND2	2.8195	159.7631
PC_166@O34	MET_1@H2	MET_1@N	2.7715	151.3087
PS_1747@O35	LYS_102@HZ3	LYS_102@NZ	2.7888	155.0644
PS_1795@O36	LYS_43@HZ1	LYS_43@NZ	2.7802	158.1306
PS_1747@O34	LYS_97@H	LYS_97@N	2.809	156.013
PE_1792@O33	ASN_103@HD21	ASN_103@ND2	2.8122	162.1384
PS_1747@O35	LYS_102@HZ2	LYS_102@NZ	2.7885	155.1419
PE_157@O12	LYS_6@HZ2	LYS_6@NZ	2.7676	154.0173
PE_1768@O22	LYS_34@HZ3	LYS_34@NZ	2.7638	150.6564
PS_1747@O36	LYS_102@HZ3	LYS_102@NZ	2.793	155.2973
PE_1729@O34	LYS_21@HZ3	LYS_21@NZ	2.7399	148.8561
PE_1768@O22	LYS_43@HZ3	LYS_43@NZ	2.7791	156.984
PE_1711@O12	LYS_45@H	LYS_45@N	2.8717	159.4827

Table 10.3. *Intermolecular Hydrogen bond analysis of membrane bound pY39 α-Syn during the MD simulation of 100 ns with pY39 α-Syn as acceptor and membrane bilayer as donor*

#Acceptor	DonorH	Donor	Average Distance (Å)	Average Angle (º)
ASN_122@OD1	PE_1744@HN1C	PE_1744@N31	2.799	154.8218
ASN_122@OD1	PE_1744@HN1B	PE_1744@N31	2.7987	155.8185
VAL_77@O	PS_1750@HN1B	PS_1750@N31	2.8284	150.7109
GLU_104@OE1	PS_1720@HN1A	PS_1720@N31	2.78	159.7195
GLN_79@OE1	PE_1735@HN1C	PE_1735@N31	2.7959	152.4059
ASP_121@OD1	PS_1813@HN1B	PS_1813@N31	2.8319	155.5349
ASP_98@OD2	PE_1708@HN1C	PE_1708@N31	2.7855	155.8524
ASP_98@OD2	PE_1708@HN1B	PE_1708@N31	2.7821	155.7837
ASP_121@OD1	PS_1813@HN1A	PS_1813@N31	2.8264	156.057
ASN_122@OD1	PE_1744@HN1A	PE_1744@N31	2.8055	154.6518
THR_81@OG1	PS_1750@HN1C	PS_1750@N31	2.8577	159.144
VAL_77@O	PS_1750@HN1A	PS_1750@N31	2.823	153.3575
GLU_104@OE1	PS_1720@HN1B	PS_1720@N31	2.7848	158.7099
VAL_77@O	PS_1750@HN1C	PS_1750@N31	2.8174	154.6191
GLU_13@OE1	PS_142@HN1B	PS_142@N31	2.7935	159.8715
GLU_13@OE1	PS_142@HN1A	PS_142@N31	2.7965	159.1261
ASP_121@OD1	PS_1813@HN1C	PS_1813@N31	2.7983	153.139
GLN_79@OE1	PE_1735@HN1A	PE_1735@N31	2.8029	152.871
ASP_115@O	PS_1843@HN1C	PS_1843@N31	2.7927	156.7298
ASP_98@OD2	PE_1708@HN1A	PE_1708@N31	2.7854	155.8661
LEU_100@O	PE_1732@HN1B	PE_1732@N31	2.7939	154.6313
GLU_130@OE2	PS_1924@HN1C	PS_1924@N31	2.7911	156.0837
ASP_121@OD2	PS_1813@HN1A	PS_1813@N31	2.8104	156.8182
GLU_137@O	PE_1726@HN1A	PE_1726@N31	2.8006	153.7729
GLU_137@O	PE_1726@HN1B	PE_1726@N31	2.8047	151.2822
ASP_121@OD2	PS_1813@HN1B	PS_1813@N31	2.7649	156.033

GLU_104@OE1	PS_1720@HN1C	PS_1720@N31	2.7892	156.9439
MET_116@O	PS_1741@HN1C	PS_1741@N31	2.8437	146.8003
GLU_137@O	PE_1726@HN1C	PE_1726@N31	2.8094	152.9362
GLU_130@OE1	PS_1924@HN1B	PS_1924@N31	2.7889	156.347
ASP_115@O	PS_1843@HN1A	PS_1843@N31	2.7773	150.5476
GLU_137@OE1	PE_1873@HN1B	PE_1873@N31	2.7727	157.3191
ASP_119@OD1	PE_1744@HN1C	PE_1744@N31	2.7832	148.4965
GLU_137@OE2	PE_1726@HN1A	PE_1726@N31	2.7491	152.3356
LEU_100@O	PE_1732@HN1C	PE_1732@N31	2.7903	154.7478
GLU_137@OE1	PE_1873@HN1A	PE_1873@N31	2.7875	157.9631
GLN_79@OE1	PE_1735@HN1B	PE_1735@N31	2.8068	152.8406
ASP_119@OD2	PE_1744@HN1C	PE_1744@N31	2.779	150.0833
ASP_119@OD2	PE_1744@HN1A	PE_1744@N31	2.7807	148.5791
GLU_105@OE1	PE_1786@HN1A	PE_1786@N31	2.7808	158.2992
GLU_83@OE2	PE_1840@HN1B	PE_1840@N31	2.8032	156.5135
GLU_105@OE1	PE_1786@HN1C	PE_1786@N31	2.8035	157.2214
ASP_121@OD2	PS_1813@HN1C	PS_1813@N31	2.8101	155.1187
LEU_100@O	PE_1732@HN1A	PE_1732@N31	2.7968	153.1469
GLU_105@OE1	PS_1720@HN1C	PS_1720@N31	2.804	157.4561
ASP_115@O	PS_1843@HN1B	PS_1843@N31	2.7808	151.543
GLN_109@OE1	PE_1786@HN1B	PE_1786@N31	2.7936	155.368
GLU_114@OE2	PE_1807@HN1C	PE_1807@N31	2.7963	155.4096
GLU_105@OE2	PS_1720@HN1C	PS_1720@N31	2.8031	158.967
GLU_46@OE1	PE_1798@HN1C	PE_1798@N31	2.7869	156.6561

Table 10.4. *Intermolecular Hydrogen bond analysis of membrane bound pS87 α-Syn during the MD simulation of 100 ns with membrane bilayer as acceptor and pS87 α-Syn as donor*

#Acceptor	DonorH	Donor	Average Distance (Å)	Average Angle (º)
PE_1798@O12	TYR_39@H	TYR_39@N	2.8244	157.791
PE_1777@O12	TYR_133@HH	TYR_133@OH	2.697	160.4173
PS_1870@O12	GLU_137@H	GLU_137@N	2.8502	156.6015
PC_1828@O34	GLN_24@HE22	GLN_24@NE2	2.8147	157.0012
PE_1780@O22	LYS_96@H	LYS_96@N	2.8713	162.4796
PC_1828@O34	LYS_58@HZ1	LYS_58@NZ	2.7559	159.5813
PS_1792@O12	ASN_103@H	ASN_103@N	2.8596	153.1087
PE_1888@O33	ASP_2@H	ASP_2@N	2.8272	156.3452
PE_1894@O33	LYS_58@HZ3	LYS_58@NZ	2.7316	159.665
PS_1837@O34	SER_42@HG	SER_42@OG	2.6161	165.599
PC_1828@O34	LYS_58@HZ2	LYS_58@NZ	2.76	160.1891
PE_1816@O34	LYS_10@HZ1	LYS_10@NZ	2.7275	158.8029
PE_1885@O12	LYS_10@HZ2	LYS_10@NZ	2.7854	159.0259
PE_1900@O22	GLY_106@H	GLY_106@N	2.8299	158.1277
PC_1828@O33	LYS_21@HZ3	LYS_21@NZ	2.7535	154.001

PC_1828@O33	LYS_21@HZ2	LYS_21@NZ	2.7403	152.511
PE_1894@O33	LYS_58@HZ1	LYS_58@NZ	2.7418	160.3052
PS_1813@O34	LYS_102@HZ1	LYS_102@NZ	2.736	157.4156
PS_1837@O33	SER_42@HG	SER_42@OG	2.6269	164.9452
PC_1828@O34	LYS_58@HZ3	LYS_58@NZ	2.7619	160.1271
PS_1804@O33	THR_59@HG1	THR_59@OG1	2.69	159.3412
PC_1828@O33	LYS_21@HZ1	LYS_21@NZ	2.7454	150.6794
PE_1843@O33	LYS_12@HZ1	LYS_12@NZ	2.7077	157.9499
PE_1780@O34	LYS_96@HZ2	LYS_96@NZ	2.7503	158.5624
PS_1813@O34	LYS_102@HZ3	LYS_102@NZ	2.7357	157.5826
PE_1843@O33	LYS_12@HZ2	LYS_12@NZ	2.734	157.8342
PS_1792@O36	LYS_102@H	LYS_102@N	2.8123	162.4881
PS_1792@O22	GLY_101@H	GLY_101@N	2.8615	157.2611
PE_1894@O33	LYS_58@HZ2	LYS_58@NZ	2.7394	160.4508
PE_1888@O11	S1P_87@H1P	S1P_87@O1P	2.8488	159.75
PE_1855@O12	LYS_34@HZ3	LYS_34@NZ	2.7697	153.9514
PE_1843@O33	LYS_12@HZ3	LYS_12@NZ	2.7319	156.8875
PE_1780@O34	LYS_96@HZ1	LYS_96@NZ	2.7548	158.9603
PE_1855@O12	LYS_34@HZ1	LYS_34@NZ	2.7687	154.2571
PE_1888@O22	S1P_87@H1P	S1P_87@O1P	2.8121	160.7947
PS_1804@O34	GLN_62@HE22	GLN_62@NE2	2.8065	160.2149
PE_1780@O33	LYS_96@HZ1	LYS_96@NZ	2.7615	158.2417
PS_1813@O34	LYS_102@HZ2	LYS_102@NZ	2.7299	157.866
PS_1795@O34	GLN_109@HE21	GLN_109@NE2	2.803	161.1589
PE_1780@O33	LYS_96@HZ3	LYS_96@NZ	2.7675	157.8328
PE_1888@O33	LYS_80@HZ3	LYS_80@NZ	2.7474	155.3416
PE_1816@O34	THR_72@HG1	THR_72@OG1	2.6514	163.7315
PS_1837@O22	LYS_43@HZ1	LYS_43@NZ	2.7631	158.6547
PC_1828@O31	GLN_24@HE22	GLN_24@NE2	2.8676	158.9188
PS_1846@O33	LYS_6@HZ1	LYS_6@NZ	2.742	158.3769
PE_1888@O33	LYS_80@HZ2	LYS_80@NZ	2.7568	155.3211
PE_1855@O12	LYS_34@HZ2	LYS_34@NZ	2.7668	153.8884
PC_1828@O22	LYS_21@HZ1	LYS_21@NZ	2.7864	152.6514
PE_1888@O12	S1P_87@H1P	S1P_87@O1P	2.7675	162.449
PE_1768@O12	GLN_134@HE22	GLN_134@NE2	2.8234	163.2147

Table 10.5. *Intermolecular Hydrogen bond analysis of membrane bound pS87 α-Syn during the MD simulation of 100 ns with pS87 α-Syn as acceptor and membrane bilayer as donor*

#Acceptor	DonorH	Donor	Average Distance (Å)	Average Angle (º)
GLU_104@OE1	PE_1765@HN1C	PE_1765@N31	2.7782	154.7345
GLU_104@OE1	PE_1765@HN1B	PE_1765@N31	2.7877	154.1973
GLU_104@OE1	PE_1765@HN1A	PE_1765@N31	2.7786	155.7706
ASP_135@OD2	PE_1786@HN1B	PE_1786@N31	2.7651	155.8698

GLU_139@OE1	PS_1879@HN1C	PS_1879@N31	2.7772	158.7379
S1P_87@O2P	PE_1780@HN1A	PE_1780@N31	2.8343	155.8446
GLU_139@OE1	PS_1879@HN1B	PS_1879@N31	2.7737	156.9231
S1P_87@O2P	PE_1780@HN1B	PE_1780@N31	2.8372	155.6062
GLU_139@OE2	PS_1879@HN1B	PS_1879@N31	2.7817	158.5138
GLU_123@OE1	PE_1852@HN1A	PE_1852@N31	2.7878	153.7639
GLU_110@OE1	PS_1957@HN1A	PS_1957@N31	2.8103	156.2245
ASP_135@OD2	PE_1786@HN1C	PE_1786@N31	2.7711	154.0292
S1P_87@O2P	PE_1780@HN1C	PE_1780@N31	2.8387	154.8519
ASP_135@OD1	PE_1786@HN1B	PE_1786@N31	2.768	155.2929
GLU_123@OE2	PE_1852@HN1A	PE_1852@N31	2.797	154.4565
TYR_136@O	PE_1768@HN1B	PE_1768@N31	2.8025	151.9161
GLU_28@OE2	PE_1855@HN1A	PE_1855@N31	2.8043	153.6774
LYS_102@O	PE_1765@HN1B	PE_1765@N31	2.8089	155.5236
GLU_131@OE2	PE_1858@HN1B	PE_1858@N31	2.7847	157.2555
GLU_123@OE1	PE_1852@HN1C	PE_1852@N31	2.7951	153.2354
GLU_123@OE1	PE_1852@HN1B	PE_1852@N31	2.7875	153.4395
GLU_139@OE2	PS_1879@HN1A	PS_1879@N31	2.782	157.859
GLU_123@OE2	PE_1852@HN1C	PE_1852@N31	2.7941	153.7191
GLU_110@OE2	PS_1957@HN1A	PS_1957@N31	2.8163	154.1094
GLU_28@OE2	PE_1855@HN1B	PE_1855@N31	2.8024	152.319
GLU_105@OE1	PS_1774@HN1C	PS_1774@N31	2.7954	155.2976
GLN_109@OE1	PS_1957@HN1C	PS_1957@N31	2.8367	158.4373
GLU_123@OE2	PE_1852@HN1B	PE_1852@N31	2.7944	153.453
GLU_139@OE1	PS_1879@HN1A	PS_1879@N31	2.7788	156.8861
GLU_104@OE2	PS_1774@HN1A	PS_1774@N31	2.7928	160.7598
ALA_140@OXT	PE_1807@HN1A	PE_1807@N31	2.7811	156.2914
ASP_135@OD1	PE_1786@HN1C	PE_1786@N31	2.7754	153.2946
GLU_28@OE1	PE_1855@HN1A	PE_1855@N31	2.8069	151.3072
ASP_135@OD2	PE_1786@HN1A	PE_1786@N31	2.7754	153.418
LYS_102@O	PE_1765@HN1C	PE_1765@N31	2.8081	154.4671
ASP_135@OD1	PE_1786@HN1A	PE_1786@N31	2.7698	153.4927
GLU_131@OE1	PE_1858@HN1B	PE_1858@N31	2.7911	155.5735
TYR_136@O	PE_1768@HN1C	PE_1768@N31	2.8119	152.3742
TYR_136@O	PE_1768@HN1A	PE_1768@N31	2.8103	151.7976
ALA_140@OXT	PE_1807@HN1C	PE_1807@N31	2.7851	156.4872
ALA_140@O	PE_1807@HN1A	PE_1807@N31	2.775	155.1993
LYS_102@O	PE_1765@HN1A	PE_1765@N31	2.8098	156.0448
ASP_121@OD2	PS_2008@HN1A	PS_2008@N31	2.7718	155.0775
GLU_28@OE1	PE_1855@HN1B	PE_1855@N31	2.8243	152.4695
GLU_83@OE2	PE_1780@HN1B	PE_1780@N31	2.7841	158.444
GLU_28@OE2	PE_1855@HN1C	PE_1855@N31	2.7997	155.0448
GLU_104@OE2	PS_1774@HN1B	PS_1774@N31	2.7885	162.3498
GLU_105@OE1	PS_1774@HN1B	PS_1774@N31	2.7859	154.3264

GLU_110@OE1	PE_1903@HN1C	PE_1903@N31	2.7821	156.9003
GLU_83@OE2	PE_1780@HN1A	PE_1780@N31	2.7791	157.9171

Table 10.6. *Intermolecular Hydrogen bond analysis of membrane bound pS129 α-Syn during the MD simulation of 100 ns with membrane bilayer as acceptor and pS129 α-Syn as donor*

#Acceptor	DonorH	Donor	Average Distance (Å)	Average Angle (º)
PS_1837@O22	LYS_43@HZ1	LYS_43@NZ	2.7789	156.9834
PS_1804@O22	LYS_21@HZ2	LYS_21@NZ	2.7645	158.901
PE_1777@O22	GLN_134@HE22	GLN_134@NE2	2.8232	158.6639
PS_1804@O22	LYS_21@HZ1	LYS_21@NZ	2.7679	158.0899
PS_1837@O22	LYS_43@HZ3	LYS_43@NZ	2.775	155.534
PS_1837@O33	SER_42@HG	SER_42@OG	2.6142	164.2168
PE_1894@O33	LYS_58@HZ1	LYS_58@NZ	2.7653	158.1616
PC_1771@O34	LYS_45@HZ2	LYS_45@NZ	2.7548	157.1366
PE_1765@O34	LYS_102@HZ3	LYS_102@NZ	2.7622	158.2354
PC_1771@O34	LYS_45@HZ1	LYS_45@NZ	2.7593	155.808
PS_1846@O34	LYS_10@HZ1	LYS_10@NZ	2.7684	159.8492
PS_1801@O34	LYS_45@HZ2	LYS_45@NZ	2.7594	158.2016
PS_1837@O22	LYS_43@HZ2	LYS_43@NZ	2.772	156.9466
PE_190@O34	MET_1@H3	MET_1@N	2.7608	157.6731
PE_1783@O22	GLN_99@HE21	GLN_99@NE2	2.8184	162.6401
PE_1885@O12	LYS_12@HZ1	LYS_12@NZ	2.7799	157.4768
PE_1885@O12	LYS_12@HZ3	LYS_12@NZ	2.783	157.718
PE_190@O34	MET_1@H2	MET_1@N	2.7449	156.8817
PE_1894@O33	LYS_58@HZ2	LYS_58@NZ	2.7721	158.6049
PS_1801@O34	LYS_45@HZ3	LYS_45@NZ	2.7714	158.2257
PE_190@O34	MET_1@H1	MET_1@N	2.7614	158.0543
PS_1804@O33	LYS_21@HZ3	LYS_21@NZ	2.7526	159.2299
PE_1894@O33	LYS_58@HZ3	LYS_58@NZ	2.7651	158.6684
PE_1888@O12	SER_87@HG	SER_87@OG	2.6761	161.1999
PE_1843@O33	LYS_80@HZ2	LYS_80@NZ	2.7485	159.244
PC_1771@O34	LYS_45@HZ3	LYS_45@NZ	2.7558	155.4823
PE_1885@O12	LYS_12@HZ2	LYS_12@NZ	2.7826	157.4235
PE_1900@O34	GLN_109@HE21	GLN_109@NE2	2.801	160.4153
PS_1804@O22	LYS_21@HZ3	LYS_21@NZ	2.7798	154.1827
PS_1831@O12	GLN_99@HE21	GLN_99@NE2	2.8218	163.7
PE_1825@O22	THR_59@HG1	THR_59@OG1	2.7015	161.5769
PS_1801@O34	LYS_45@HZ1	LYS_45@NZ	2.7659	156.884
PE_1765@O34	LYS_102@HZ1	LYS_102@NZ	2.7513	159.0935
PE_1843@O34	LYS_80@HZ2	LYS_80@NZ	2.7492	159.3872
OL_1863@H9R	TYR_39@H	TYR_39@N	2.8225	155.0978
PE_1834@O34	LYS_80@HZ1	LYS_80@NZ	2.693	159.5133
PC_1771@O22	LYS_45@HZ3	LYS_45@NZ	2.7613	152.587

PE_1765@O34	LYS_102@HZ2	LYS_102@NZ	2.7648	158.2706
PS_1822@O34	VAL_118@H	VAL_118@N	2.8599	155.6457
PS_1804@O33	LYS_21@HZ2	LYS_21@NZ	2.7673	161.9166
PS_1813@O36	LYS_102@HZ2	LYS_102@NZ	2.7773	155.4121
PE_1900@O33	GLN_109@HE21	GLN_109@NE2	2.7857	161.8982
PE_1768@O22	TYR_133@HH	TYR_133@OH	2.7099	157.034
PC_1828@O22	LYS_23@HZ2	LYS_23@NZ	2.7628	158.4227
PS_1792@O33	ASN_103@HD21	ASN_103@ND2	2.8009	163.7393
PC_1771@O22	LYS_45@HZ2	LYS_45@NZ	2.7727	152.9171
PE_1834@O12	LYS_80@HZ3	LYS_80@NZ	2.7813	155.4032
PS_1801@O12	LYS_45@HZ1	LYS_45@NZ	2.7643	156.8611
PC_1828@O22	LYS_23@HZ3	LYS_23@NZ	2.756	157.7348
PS_1831@O35	ASP_98@H	ASP_98@N	2.8078	160.1896

Table 10.7. *Intermolecular Hydrogen bond analysis of membrane bound pS129 α-Syn during the MD simulation of 100 ns with pS129 α-Syn as acceptor and membrane bilayer as donor*

#Acceptor	DonorH	Donor	Average Distance (Å)	Average Angle (º)
GLU_137@OE2	PE_1786@HN1B	PE_1786@N31	2.7983	157.4517
PRO_138@O	PE_1768@HN1A	PE_1768@N31	2.8027	154.551
PRO_117@O	PE_1852@HN1A	PE_1852@N31	2.798	156.9147
PRO_117@O	PE_1852@HN1C	PE_1852@N31	2.7973	156.652
PRO_117@O	PE_1852@HN1B	PE_1852@N31	2.7998	156.6421
GLU_123@OE2	PE_1852@HN1C	PE_1852@N31	2.7787	157.8293
GLU_137@OE1	PE_1786@HN1B	PE_1786@N31	2.7932	153.1936
GLN_134@O	PE_1786@HN1A	PE_1786@N31	2.8186	151.5001
GLU_123@OE2	PE_1852@HN1B	PE_1852@N31	2.7783	159.1843
TYR_136@O	PE_1768@HN1C	PE_1768@N31	2.7895	150.985
GLU_104@OE1	PS_1915@HN1A	PS_1915@N31	2.803	156.8188
TYR_136@O	PE_1768@HN1A	PE_1768@N31	2.7865	150.6246
PRO_138@O	PE_1768@HN1B	PE_1768@N31	2.8002	154.3914
GLU_137@OE2	PE_1786@HN1C	PE_1786@N31	2.7822	156.9373
GLU_104@OE2	PE_1765@HN1B	PE_1765@N31	2.7716	154.8893
GLU_104@OE2	PE_1765@HN1C	PE_1765@N31	2.7821	155.0939
GLU_139@OE1	PE_1807@HN1A	PE_1807@N31	2.7687	156.6894
GLU_104@OE2	PE_1765@HN1A	PE_1765@N31	2.7825	155.0699
ASP_115@O	PE_1900@HN1B	PE_1900@N31	2.8226	151.346
PRO_138@O	PE_1768@HN1C	PE_1768@N31	2.8008	152.3511

ASP_115@OD2	PE_1903@HN1A	PE_1903@N31	2.8196	156.1322
ASP_115@OD2	PE_1903@HN1B	PE_1903@N31	2.8159	154.1626
GLU_123@OE2	PE_1852@HN1A	PE_1852@N31	2.7931	156.5802
ASP_115@OD1	PE_1903@HN1B	PE_1903@N31	2.813	153.2582
GLU_114@O	PE_1900@HN1B	PE_1900@N31	2.801	149.3946
GLU_137@OE2	PE_1786@HN1A	PE_1786@N31	2.7908	156.6718
GLN_134@O	PE_1786@HN1B	PE_1786@N31	2.8126	150.5957
ASP_135@O	PE_1786@HN1A	PE_1786@N31	2.8276	152.8067
GLU_104@OE1	PS_1915@HN1C	PS_1915@N31	2.8094	156.2048
GLU_83@OE1	PE_1888@HN1A	PE_1888@N31	2.7965	156.0684
ASP_115@OD1	PE_1903@HN1A	PE_1903@N31	2.8164	152.3484
GLU_137@OE1	PE_1786@HN1C	PE_1786@N31	2.7993	152.1529
TYR_136@O	PE_1768@HN1B	PE_1768@N31	2.7894	150.3598
ASP_115@O	PE_1900@HN1C	PE_1900@N31	2.8235	151.7766
GLU_137@OE1	PE_1786@HN1A	PE_1786@N31	2.7868	150.9608
GLU_139@OE1	PE_1807@HN1B	PE_1807@N31	2.7811	156.9606
GLU_114@O	PE_1900@HN1C	PE_1900@N31	2.7938	151.1362
GLU_110@OE2	PE_1903@HN1C	PE_1903@N31	2.7958	158.0293
GLU_105@OE1	PS_1774@HN1A	PS_1774@N31	2.7924	156.4394
ASP_115@OD1	PE_1903@HN1C	PE_1903@N31	2.8051	151.8857
ASP_98@O	PE_1783@HN1C	PE_1783@N31	2.8244	154.4385
GLU_83@OE1	PE_1888@HN1C	PE_1888@N31	2.8082	156.7198
GLN_134@O	PE_1786@HN1C	PE_1786@N31	2.8151	149.6019
GLU_131@OE1	PE_1858@HN1B	PE_1858@N31	2.7739	154.4126
GLU_83@OE1	PE_1888@HN1B	PE_1888@N31	2.8035	156.5578
GLU_139@OE1	PE_1807@HN1C	PE_1807@N31	2.7773	155.3836
GLU_114@O	PE_1900@HN1A	PE_1900@N31	2.8017	151.5322
GLU_104@OE1	PS_1915@HN1B	PS_1915@N31	2.8164	155.9016
GLN_109@OE1	PS_1774@HN1A	PS_1774@N31	2.8111	157.2662
ASP_98@O	PE_1783@HN1B	PE_1783@N31	2.8312	154.6478

10.4.10. Hydrogen bond Analysis within phosphorylated α-Synuclein complexes:

Additionally, the analysis of Hydrogen bond analysis within the different regions phosphorylated α-Syn was carried out. Although the NAC and C-terminal regions were found

to contain lower hydrogen bond interactions, the results obtained in **Figures 10.18-10.20** demonstrated stronger intramolecular contacts between the N-terminal and NAC regions. Within the various areas, intramolecular hydrogen bond interactions act as an important role in the structural compactness of pS129 α-Syn.The number of hydrogen bond formation between different domains of phosphorylated α-Syn were analyzed to determine the proximity within the domains of the protein**.** From the results observed, the intra-molecular hydrogen bonds within the N-terminal region (1–60), NAC domain (61–95), and C-terminal region (96–140) of both the phosphorylated systems showed slight dissimilarity. The N-terminal domain of pS87 α-Syn showed subtle fluctuation in the number of hydrogen bonds during the simulation while pY39 α-Syn maintained its slope throughout the simulation.

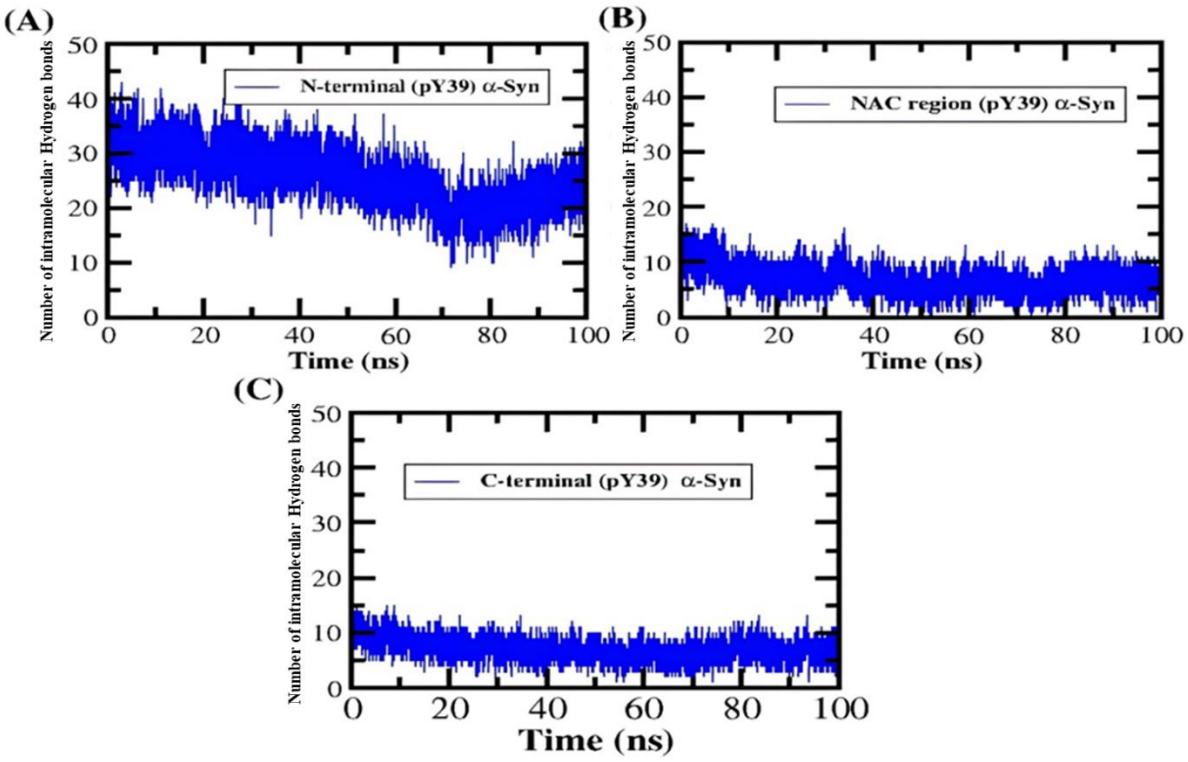

Figure 10.18. *Intramolecular of the phosphorylated α-Syn (A) N-terminal, (B) NAC region, and (C) C-terminal of the phosphorylated α-Syn pY39 during MD simulation*

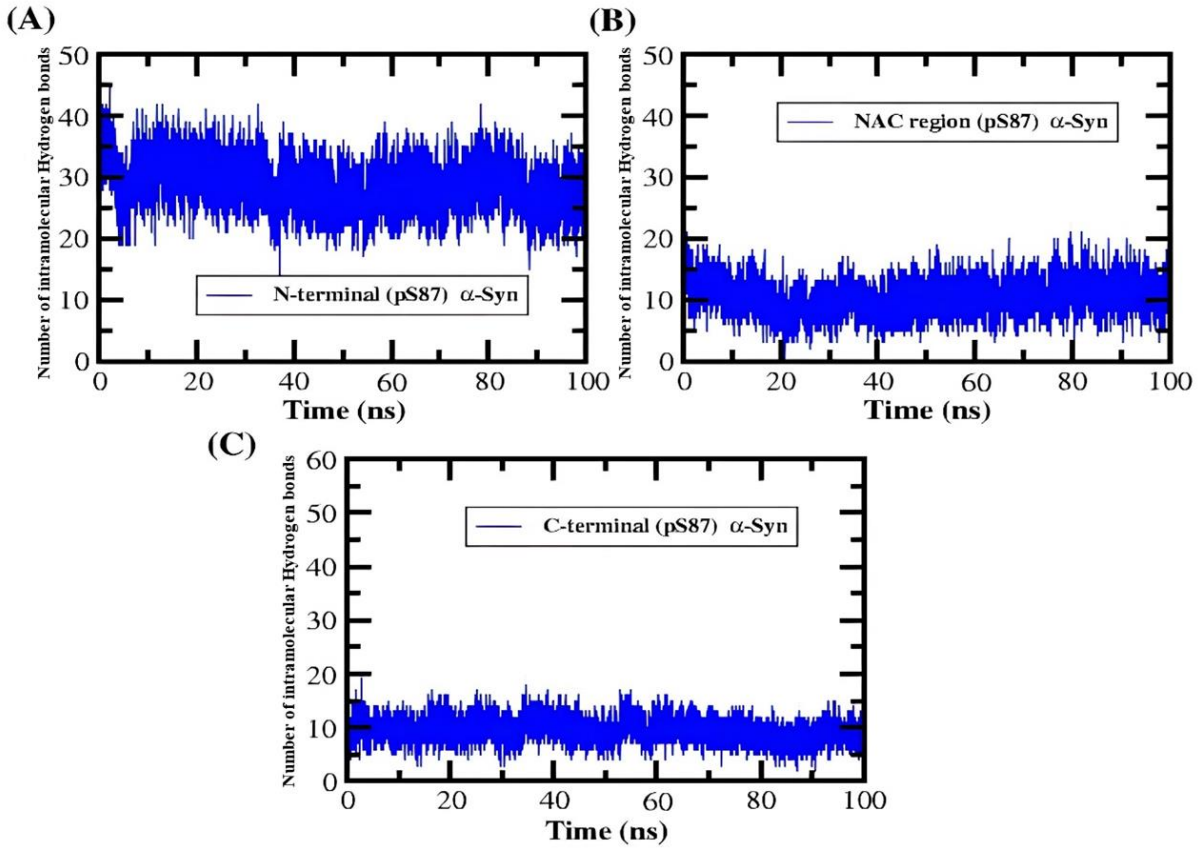

Figure 10.19. *Intramolecular of the phosphorylated α-Syn (A) N-terminal, (B) NAC region, and (C) C-terminal of the phosphorylated α-Syn pS87 during MD simulation*

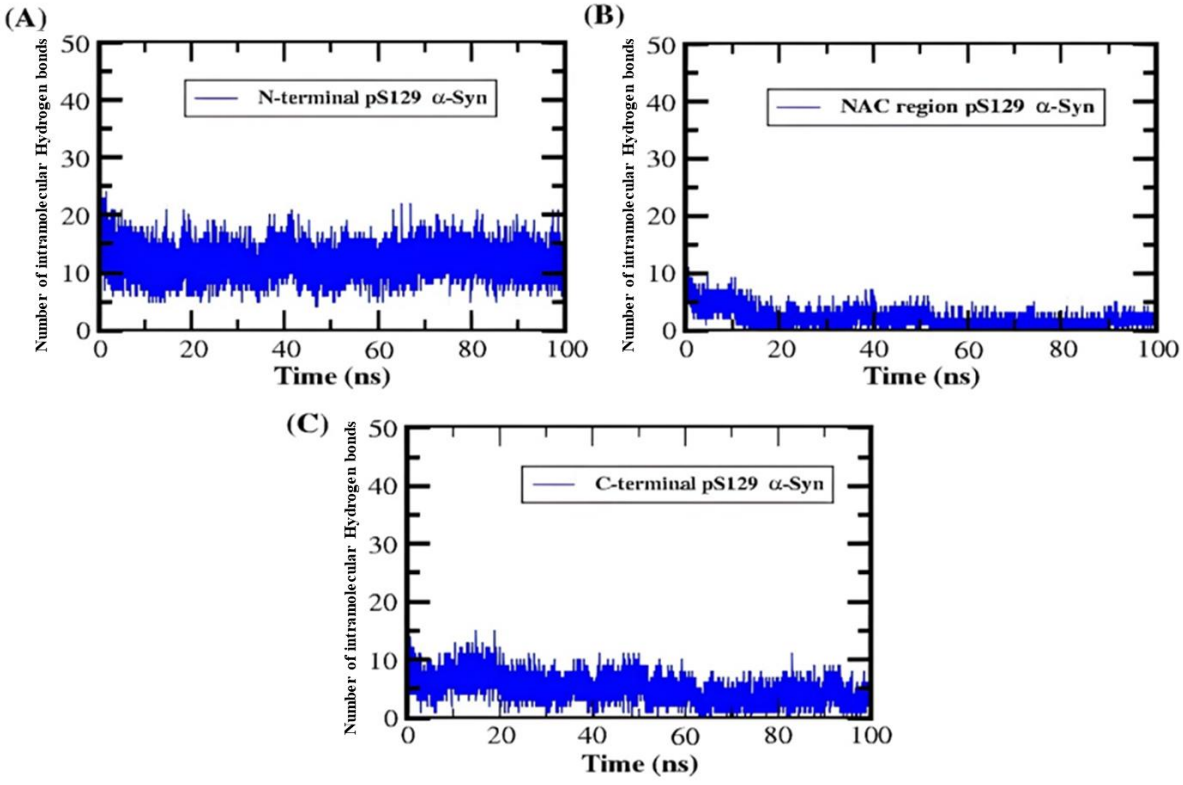

Figure 10.20. *Intramolecular of the phosphorylated α-Syn (A) N-terminal, (B) NAC region, and (C) C-terminal of the phosphorylated pS129 α-Syn during MD simulation*

10.4.11. Phosphorylated α-Synuclein complexes stabilizes salt bridge formation:

To ensure the stability of pY39, pS87 and pS129 α-Syn, the number of salt bridges and their distance within the N-terminal, NAC, and C-terminal regions of the α-Syn were determined. Understanding the dynamics and impact of salt bridge formation provides valuable insights into protein-protein interactions, ligand binding, and enzymatic activity, contributing to the broader understanding of molecular biology and facilitating the design of novel therapeutics targeting specific protein functions [646]. The formation of salt bridges is one of the characteristics of the fibril, as are the various intramolecular interactions that maintain the structural conformity of pY39, pS87 and pS129 α-Syn. Using the ESBRI server, the list of residue-residue interactions and the distance in (Å) within the N-terminal, NAC region, and C-terminal of the pS129 α-Syn interface were evaluated [644]. It was observed that the stability of the α-Syn on phosphorylation at residue 129 involved 11 strong intra-monomeric salt bridge formations, as summarized in **Table 10.8**. From the **Table 10.9** and **Table 10.10**, the number of salt bridges was found to be higher in pS87 α-Syn as compared to pY39 α-Syn. the majority of the salt bridge formation occurred between Lysine (Lys) residues and Glutamine (Glu) residues of the N-terminal domain in both the phosphorylated systems. Therefore, the number of salt bridges formed are considered a key characteristic of the monomeric structures that includes various interactions within the molecules to stabilize the α-Syn structure. Also, it has been reported in a study [647] that the formation of salt bridge (E46-K80) between the monomeric units in the fibrils plays a crucial role in stabilization and maintaining hydrophobic interactions between the protofibrils. From the analysis, it can also be noted that a higher number of salt bridges were formed within the N-terminal as compared to other regions, which suggests the conformational stability of the region. Therefore, the formation of salt bridges within the N-terminal region suggests stabilization of the pS129 α-Syn.

Table 10.8. *List of atom-atom interactions within the pY39 interface from the ESBRI server*

α-Syn (pY39) (Residue 1)				Hydrogen Bonds	α-Syn (pY39) (Residue 2)				
Atom number	Atom name	Residue name	Residue number		Atom number	Atom name	Residue name	Residue number	Distance (Å)
113.6	NZ	LYS	10	<-->	111.8	OE1	GLU	13	4
106.7	NZ	LYS	12	<-->	111.8	OE1	GLU	13	1.94
106.5	NZ	LYS	23	<-->	107.4	OE1	GLU	20	3.45

97.4	NZ	LYS	32	<-->	99.6	OE1	GLU	28	2.04
97.4	NZ	LYS	32	<-->	99	OE1	GLU	35	2.47
81.7	NZ	LYS	102	<-->	88.6	OE1	GLU	105	2.55

Table 10.9. *List of atom-atom interactions within the pS87 interface from the ESBRI server*

α-Syn (pS87) (Residue 1)				Hydrogen Bonds	α-Syn (pS87) (Residue 2)				
Atom number	Atom name	Residue name	Residue number		Atom number	Atom name	Residue name	Residue number	Distance (Å)
111.6	NZ	LYS	23	<-->	110	OE1	GLU	20	2.25
100.6	NZ	LYS	32	<-->	104.4	OE1	GLU	35	2.58
104.4	NZ	LYS	43	<-->	104.4	OE1	GLU	35	2.90
104.8	NZ	LYS	58	<-->	105.5	OE1	GLU	28	2.73
93.62	NZ	LYS	60	<-->	94.7	OE1	GLU	57	2.50
91.09	NZ	LYS	102	<-->	97.2	OD1	ASP	98	2.29
91.09	NZ	LYS	102	<-->	96	OD2	ASP	98	3.99

Table 10.10. *List of atom-atom interactions within the pS129 interface from the ESBRI server*

pS129 α-Syn (Residue 1)				Hydrogen Bonds	pS129 α-Syn (Residue 2)				
Atom number	Atom name	Residue name	Residue number		Atom number	Atom name	Residue name	Residue number	Distance (Å)
112	NZ	LYS	6	<-->	110	OD1	ASP	2	3.43
112	NZ	LYS	6	<-->	110	OD2	ASP	2	1.54
108	NZ	LYS	10	<-->	114	OE1	GLU	13	2.73
105	NZ	LYS	21	<-->	113	OE1	GLU	20	0.94
116	NZ	LYS	23	<-->	113	OE1	GLU	20	1.84
116	NZ	LYS	23	<-->	115	OE1	GLU	61	2.44
109	NZ	LYS	34	<-->	108	OE1	GLU	35	2.61
110	NZ	LYS	43	<-->	108	OE1	GLU	35	3.67
112	NZ	LYS	58	<-->	111	OE1	GLU	28	2.57
96	NZ	LYS	102	<-->	98	OD1	ASP	98	0.50
96	NZ	LYS	102	<-->	100	OD2	ASP	98	1.67

10.4.12. Distance Analysis of phosphorylated α-Synuclein complexes:

The center of mass distance between the N-terminal domain and C-terminal domain of phosphorylated (pS87 and pY39) α-Syn as a function of simulation time were analyzed in **Figure 10.21**. The distance between the N-terminal domain and the C-terminal domain of pY39 α-Syn was observed to be higher than pS87 α-Syn. The slight decrease in the center of mass distance between the two domains of pS87 α-Syn correlates to the higher bending of the conformation resulting in the exposure of the N-terminal domain from the membrane bilayer.

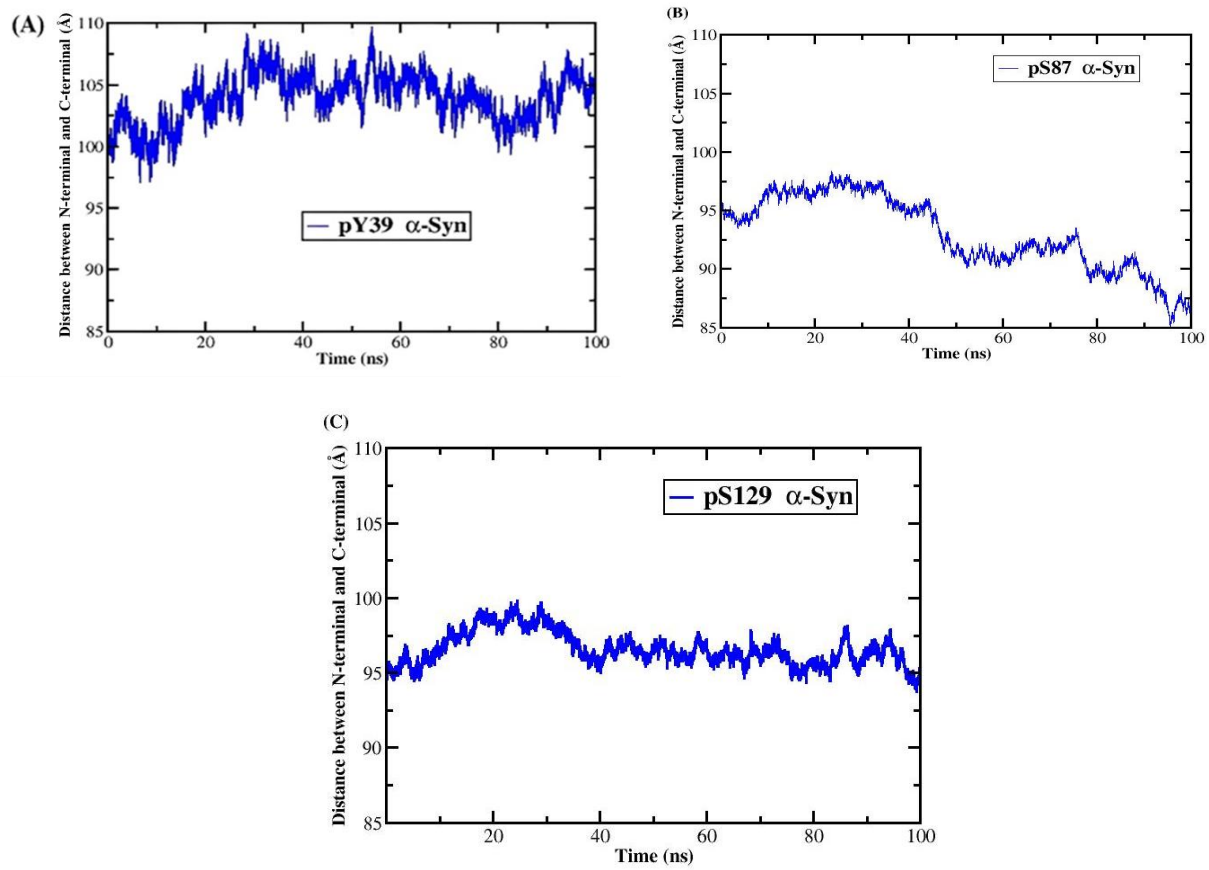

Figure 10.21. *Distance analysis of the phosphorylated α-Syn (A) pY39, (B) pS87and (C) pS129 during MD simulation*

10.5. Conclusion:

In this study, the focus is on the effect of phosphorylation (pY39, pS87 and pS129) on the conformational dynamics of α-Syn in association with lipid membrane using all-atom MD simulations were performed. The significance of the study is the pY39 showing conformational fluctuations that causes high degree of fluctuations in the N-terminal region that disrupts the helix-2 binding region while the pS87 α-Syn determines the flanking of the C-terminal from the membrane that aids in decreased binding affinity towards the membrane bilayer. The impact of this study demonstrates that Phosphorylation can induce structural alterations in α-Syn. Tyrosine and Serine phosphorylation can introduce bulky phosphate groups, which may disrupt local protein conformation or promote interactions with other molecules. Phosphorylation at Tyr39 and Ser87 may modulate the protein's aggregation propensity, either promoting or inhibiting the formation of toxic aggregates. Phosphorylation can alter protein-protein interactions involving α-Syn. Phosphorylated residues may serve as binding sites for other proteins or modify existing interaction interfaces, thereby influencing signalling pathways or protein complex formation. Understanding the impact of phosphorylation on α-

Syn could identify potential therapeutic targets for neurodegenerative diseases.The stabilization of the membrane bilayer system was determined in the range of ±20 Å, which is considered to be well equilibrated. The density profile for each components of the membrane bilayer and individual domains of the phosphorylated α-Syn structures were analysed. Based on the electron density profiles, the pY39 α-Syn showed higher insertion of N-terminal domain below the bilayer center as compared to pS87 α-Syn and pS129 α-Syn. The binding environment of pS129 α-Syn was significantly changed, resulting in Helix-N being buried deeper beneath the head group phosphates of the lipid bilayer. MD simulation trajectory analyses such as RMSD and R_g profile suggest stability and compactness of the pY39, pS87 and pS129 α-Syn. The stability of pY39 and pS87 α-Syn were determined by RMSD and RMSF profiles, where it was noticed that pS87 showed higher flexibility and fluctuation during the MD simulation. Also, the 3-D and 2-D plots of PCA analysis showed pY87 α-Syn to have maximum lowest energy and deeper basins as compared to pY39 which correlates with the RMSD lowest energy of the overall structure. PCA and free energy landscape exhibited global minima of pS129 α-Syn. In an aqueous environment, hydrophobic and hydrophilic sidechain rearrangements were used to generate the ideal backbone shape for structural stability by means of optimum water interactions [635]. Similarly, our study showed that the NAC region of pS129 α-Syn shows higher flexibility as it is found to emerge from the lipid membrane. It was noticed that the residues (71-82) of the NAC region showed the absence of α-strand as carbonyl groups and amino groups are located on both sides of the chain rather than oriented on one side forming an α-strand. The RMSD of all the Cα atoms was plotted and obtained from the MD trajectories using the lowest energy structure as a reference initial structure to analyze the folding pattern with respect to time. The RMSD plot showed fluctuations after 80 ns time suggesting phosphorylated pS129 α-Syn undergo a unique folding pattern. From the percentage secondary structural content analysis, it was found that pS129 α-Syn and pS87 α-Syn predominantly contains higher α-helix that helps in better stability of the system while the higher coil and turn content were observed in the pY39 α-Syn. The conformational snapshots of the α-Syn indicated that pY39 α-Syn undergo fluctuation near the site of Tyr39 as a result a disruption of helix-2 binding region occurs and in the case of pS87 α-Syn, due to the phosphorylation the C-terminal is flanked out of the membrane that aids in decreased binding affinity towards the membrane bilayer. Om the contrary, pS129 α-Syn was noticed that the N-helix is beneath the membrane bilayer, the NAC hydrophobic area rises above the bilayer, and the C-terminal has limited membrane contact. The hydrogen bond analysis between pS129 α-Syn (N-terminal and NAC region) and lipid membrane showed decreasing interaction

suggesting pS129 introduces additional negative charges that impart subtle changes in their interactions. The intra-molecular hydrogen bond interaction within the NAC region and N-terminal, NAC region, and C-terminal were analyzed. In the case of the NAC region and N-terminal, a higher intra-molecular hydrogen bonds interaction was observed than the NAC and C-terminal region due to the presence of a phosphate group at residue 129. Several studies reported that interaction of α-Syn with monovalent, divalent and trivalent ions may promote fibrillation of α-Syn [648]. Several research studies reveal the presence of an intra-molecular salt-bridge that aids in the assembly of aggregated fibril structure [303]. Also, a higher occurrence of salt bridges was noticed within the N-terminal region than in the NAC region followed by the C-terminal of pS129 α-Syn. Our findings emphasize the effect of phosphorylated pS129 on the conformational structure of α-Syn and its interaction with the lipid membranes. This MD simulation study provided light on the function of phosphorylation at Serine 129, which can stabilize the protein's propensity to adopt an α-helical rich shape by reducing the hydrophobicity of binding sites. Interestingly, our findings also demonstrate that pS87 phosphorylation changes the conformation of α-Syn and reduces its affinity for lipid vesicles. This is likely due to the α-Syn protein's decreased lipid-binding affinity surrounding the phosphorylation site and instability of the helical conformation.Therefore, pY39 α-Syn contributed to the initiation of aggregates by disrupting the helix-2 binding site and initiate in the unfolding of the α-Syn structure.